

The Luttinger-Kohn theory for multiband Hamiltonians: A revision of ellipticity requirements

Dmytro Sytnyk*

*Numerical Mathematics Department. Institute of Mathematics, National Academy of Sciences, Ukraine;
M²NeT Laboratory, Wilfrid Laurier University, 75 University Avenue West, Waterloo, ON, Canada, N2L 3C5.*

Roderick Melnik†

M²NeT Laboratory, Wilfrid Laurier University, 75 University Avenue West, Waterloo, ON, Canada, N2L 3C5.

Modern applications require a robust and theoretically solid tool for the realistic modeling of electronic states in low dimensional nanostructures. The $k \cdot p$ theory has fruitfully served this role for the long time since its establishment. During the last three decades several problems have been detected in connection with the application of the $k \cdot p$ approach to such nanostructures. These problems are closely related to the violation of the ellipticity conditions for the underlying model, the fact that has been largely overlooked in the literature. We derive ellipticity conditions for 6×6 , 8×8 and 14×14 Hamiltonians obtained by the application of Luttinger-Kohn theory to the bulk zinc blende (ZB) crystals, and demonstrate that the corresponding models are non-elliptic for many common crystalline materials. With the aim to obtain the admissible (in terms of ellipticity) parameters, we further develop and justify a parameter rescaling procedure for 8×8 Hamiltonians. This allows us to calculate the admissible parameter sets for GaAs, AlAs, InAs, GaP, AlP, InP, GaSb, AlSb, InSb, GaN, AlN, InN. The newly obtained parameters are then optimized in terms of the bandstructure fit by changing the value of the inversion asymmetry parameter B that is proved to be essential for ellipticity of 8×8 Hamiltonian. The consecutive analysis, performed here for all mentioned $k \cdot p$ Hamiltonians, indicates the connection between the lack of ellipticity and perturbative terms describing the influence of out-of-basis bands on the structure of the Hamiltonian. This enables us to quantify the limits of models' applicability material-wise and to suggest a possible unification of two different 14×14 models, analysed in this work.

PACS numbers: 71.20.-b, 71.20.Nr, 73.22.-f, 31.15.xp, 02.30.Jr

I. INTRODUCTION

The collection of methods known as an effective mass theory is one of the fundamental topics in the physics of nanostructures. The theory has been used to describe a wide variety of physical phenomena ranging from the formation of electronic bands in periodic solids to the realistic field-matter interaction in modern semiconductor materials. Furthermore, the theory establishes a robust computational framework for simulating observable quantum-mechanical states and corresponding energies in the low-dimensional nanoscale systems, including quantum wells, wires and dots.

In the original Luttinger-Kohn work¹ authors applied the perturbation theory to the Schrödinger equation with a smooth potential and constructed a representation for valence bands Hamiltonian near the high symmetry point Γ of the first Brillouin zone in bulk zinc blende (ZB) crystals with large fundamental bandgap. Soon after that, Kane showed how to extend the model to the narrow gap materials such as InSb and Ge for instance, where one can also account for the influence of the conduction bands². One of the advantages of the $k \cdot p$ theory is in its universality and flexibility when it comes to simulation of electronic transport phenomena in the presence of electromagnetic and/or thermoelastic fields^{3,4}. Indeed, the theory had also been extended to cover Wurtzite (WZ) type of crystals, materials with inclusions, heterostruc-

ture materials and superlattices⁵⁻⁷. Another advantage of the effective mass theory is its flexibility, as one can easily adjust the models to include additional effects like strain⁸, piezoelectricity, magnetic field, and respective nonlinear effects. These inbuilt multiscale effects are crucial for such applications as light-emission diodes, lasers, high precision sensors, photo-galvanic elements, hybrid bio-nanodevices, and many others⁹.

For a wide range of applications the Luttinger-Kohn models have provided good, computationally feasible and efficient approximations that agree well with experimental results^{10,11}. However, for some types of crystal materials band structure calculations based on such multiband models lead to the solutions with unphysical properties^{12,13} or so called spurious solutions¹⁴⁻¹⁹.

As a result, there have been various attempts to explain the origin of the spurious solutions and develop some reliable procedures on how to avoid them^{16,19-21}. These approaches rely on three main ideas: (a) to modify the original Hamiltonian and remove the terms responsible for the spurious solutions^{15,22}, (b) to change bandstructure parameters^{14,20,23}, and (c) to identify and exclude from simulations the physically inadequate observable states^{11,24} or change the numerical scheme to avoid such states altogether^{21,25}. All mentioned approaches suffer from the common weakness – the lack of clear justification of the underlying theoretical procedure and thus from limitations in their applicability^{16,17}.

In this work we show that spurious solutions are just a consequence of a more fundamental problem in applications of the effective mass theory: the non-ellipticity of the multiband Hamiltonian in the position representation.

The systematic study of connection between the structure of 6×6 , 8×8 and 14×14 Hamiltonians, their ellipticity in the position representation and the material parameters for ZB crystals allow us to conclude that the widely adopted $k \cdot p$ models turn out to be non-elliptic (hyperbolic) for a broad class of known material parameters. The phase space of the hyperbolic model is wider than the spaces of norm-bounded observable states. Such models, therefore, are susceptible to unphysical solutions, even in the bulk case. Meanwhile, the corresponding time-dependent Schrödinger equation loses the fundamental property of state conservation²⁶.

These facts lead to an important assertion. Since any qualitative multiband approximation of Schrödinger Hamiltonian must preserve its core physical properties, such as ellipticity and, as a consequence, semi-boundedness of set of energy states; the lack of ellipticity for certain materials implies that the usage of multiband Hamiltonian for such materials is fundamentally incorrect. This results in substantial ramifications for the applications of effective-mass theory to bulk solids and heterostructures.

The whole procedure of obtaining the materials parameters from experiment and their incorporation into mathematical models of effective mass theory needs to be revisited, taking into account the general ellipticity constraints derived in the present work. Before this is done, we propose here the sets of elliptic Hamiltonian parameters for GaAs, AlAs, InAs, GaP, AlP, InP, GaSb, AlSb, InSb, GaN, AlN, InN, optimized in terms of the bandstructure fit. We also supply a parameter rescaling procedure used to obtain these sets from the available non-elliptic parameters.

The paper is organized as follows. First, we revise basic properties of the Schrödinger equation and its approximations represented by $k \cdot p$ models. In section III we outline a mathematical procedure to obtain the ellipticity constraints for a Hamiltonian in the position representation. For the $k \cdot p$ Hamiltonians the constraints are comprised of the set of linear material-dependent inequalities²⁷. In sections III and IV we present a direct evaluation of ellipticity constraints for 6×6 and 8×8 ZB Hamiltonians based on parameter sets gathered from major material-data sources^{28–32}. Most of the 53 analyzed parameter sets lead to the failure of the Hamiltonians' ellipticity. That is why the main part of section IV is devoted to a parameter rescaling procedure aimed at correcting the Hamiltonian's ellipticity. As a result of the procedure we propose elliptic parameter sets for all analyzed materials. The newly obtained sets are, then, compared to the original materials parameters by means of the differences in the associated bandstructures of 8×8 Hamiltonian. In this section, we further extend

the ellipticity conditions of 8×8 model³³ to the case of nonzero inversion-asymmetry parameter B . Afterwards, B is used to improve the bandstructure fit of the proposed elliptic parameter set for indium nitride. Section V is devoted to the ellipticity analysis of two existing 14×14 models^{34,35}.

The summary of results together with discussions on applicability and future directions are given in the concluding section.

II. OVERVIEW OF LUTTINGER-KOHN BANDSTRUCTURE THEORY

The material properties (such as fundamental bandgaps and spin-orbit splitting energies) obtained experimentally, represent real quantum phenomena, whereas models based on multiband Hamiltonians are meant to approximate them. As such these models are derived from the stationary Schrödinger equation that represents an averaged charge carrier interactions in the crystalline structure^{36,37}. The derivation scheme involves the application of Bloch wave representation and the projection of the original Hamiltonian to the orthogonal subspace of the reduced phase space^{1,38}. The projective part of Hamiltonian is then adjusted with help of perturbation theory^{1,38,39} to account for the influence of outer bands. However, this last step lacks a rigorous theoretical foundation as it does not guarantee the convergence of the perturbative expansion^{40,41}. The result is that the derived Hamiltonian, although directly based on the experimental parameters (Tables I, II, V), represents a totally different mathematical object compared to its origin. The physical evidence, to support this claim has been already known for GaAs⁴² and for Si⁴³.

We start with the Schrödinger equation

$$H_0\psi(x) \equiv \left(\frac{\mathbf{p}^2}{2m_0} + V(x) + H_{SO} \right) \psi(x) = E_n\psi(x), \quad (1)$$

where $\mathbf{p} = i\hbar\nabla$ is a momentum operator of charge carrier with the mass m_0 , $V(x)$ is the effective potential, $x \in \Omega \subset \mathbb{R}^3$. The unknown E_n , stands for the eigenenergy of the system and the function $\psi(x)$ is the corresponding eigenstate. The Hamiltonian H_{SO} accounts for relativistic effects of spin.

In the finite domain Ω we supplement (1) by the boundary conditions

$$\psi(x) = f(x), \quad x \in \partial\Omega, \quad (2)$$

assuming that the combination of given Ω and $f(x)$ endows operator H_0 with all necessary properties, postulated by the standard axiomatic approach to quantum mechanics⁴⁴. The operator H_0 is an elliptic partial differential operator. It is symmetric over its domain of definition $D(H_0) \subset \mathcal{H}^3(\Omega)$. Furthermore we require that the boundary $\partial\Omega$ is sufficiently smooth, so that a self-adjoint extension of H_0 exists and possesses the property of the

probability current conservation^{44,45}. All mentioned assumptions can be satisfied in the bulk case⁴⁶, which will be our main focus throughout the work.

If $V(x)$ is a gently varying function over the unit cell¹, the original operator H_0 can be approximated by another operator H (using Bloch theorem), determined by the projection P of H_0 on the considered eigenspace and Löwdin perturbation theory^{1,38}. The last step in this approximation procedure accounts for the influence of the elements from the space (so-called class of states B) complement to the chosen eigenspace (so-called class of states A) by the formula

$$H = PH_0 + \sum_{i=1}^r \delta^i H^{(i)} \quad (3)$$

up to the order r . Setting $\delta = 1$ leads one to the final approximation, under the assumption that the series (3) is convergent for such δ . Despite wide applicability of such

approximations, the intrinsic ellipticity requirements for the realizations of H have not been explicitly verified in a systematic manner (see 1, 2, 20, 38, and 47, as well as more recent works^{14,15,18,22,25,34,35}). The only known to us work where it has been done for the case of InAs, GaAs and $\text{Al}_{0.3}\text{Ga}_{0.7}\text{As}$ is [16]. Hence, in what follows we analyze such requirements systematically for all common 6×6 , 8×8 and 14×14 ZB Hamiltonians.

III. SIX-BANDS HAMILTONIAN ANALYSIS

This section is devoted the ellipticity analysis of the classical 6×6 Hamiltonian for ZB¹ type of crystals, demonstrating our approach in detail. In this work we use the Luttinger parameter notation which is common in recent works on the subject. When necessary, the parameters will be converted from other parameter notations³⁷

The Luttinger-Kohn (LK) Hamiltonian is defined as follows^{38,39}

$$H^{LK} = \begin{pmatrix} P+Q & S & R & 0 & -\frac{1}{\sqrt{2}}S & -\sqrt{2}R \\ S^* & P-Q & 0 & R & \sqrt{2}Q & \sqrt{\frac{3}{2}}S \\ R^* & 0 & P-Q & -S & \sqrt{\frac{3}{2}}S^* & -\sqrt{2}Q \\ 0 & R^* & -S^* & P+Q & \sqrt{2}R^* & -\frac{1}{\sqrt{2}}S^* \\ -\frac{1}{\sqrt{2}}S^* & \sqrt{2}Q & \sqrt{\frac{3}{2}}S & \sqrt{2}R & P-\Delta_{SO} & 0 \\ -\sqrt{2}R^* & \sqrt{\frac{3}{2}}S^* & \sqrt{2}Q & -\frac{1}{\sqrt{2}}S & 0 & P-\Delta_{SO} \end{pmatrix} \quad \begin{aligned} P &= -\frac{\hbar^2}{2m_0}\gamma_1\mathbf{k}^2, \\ Q &= -\frac{\hbar^2}{2m_0}\gamma_2(k_x^2 + k_y^2 - k_z^2), \\ R &= -\frac{\hbar^2}{2m_0}\frac{-\sqrt{3}}{2}[(\gamma_2 + \gamma_3)k_-^2 + (\gamma_2 - \gamma_3)k_+^2], \\ S &= -\frac{\hbar^2}{2m_0}(-2\sqrt{3})\gamma_3k_-k_z, \end{aligned}$$

where $\mathbf{k}^2 = k_x^2 + k_y^2 + k_z^2$, $k_{\pm} = k_x \pm ik_y$. Each of the P, Q, R, S is a second order position dependent differential operator in the position representation or, equivalently, second order polynomial in the momentum representation¹.

Our aim is to check the type (elliptic, hyperbolic or essentially hyperbolic) of the H^{LK} as a partial-differential operator (PDO), keeping in mind that the Schrödinger operator from (1) is elliptic. Only the second order derivative terms are playing the dominant role in the following analysis because contributions from the terms linear in the components of \mathbf{k} as well as from the potential, are bounded in the domain $D(H^{LK})$ ⁴⁸. It means that the results for more complicated physical models with potential contributions from additional fields (e.g. strain, magnetic field, etc.) will stay the same as for the original H^{LK} , analyzed here. The fact that the Hamiltonian is a linear operator guarantees that it is also true for any other representation of H^{LK} obtained by linear (basis) transformations.

In a more general sense, for any m -dimensional matrix PDO $H = \{h_{ij}\}_{i,j=1}^m$, where each element h_{ij} is a second

order one-dimensional PDO^{49,50}

$$h_{ij} = \sum_{k,l=0}^n h_{ij}^{kl} \frac{\partial^2}{\partial x_k \partial x_l}, \quad (4)$$

the associated quadratic form (also known in the mathematical literature as a principal symbol) is defined by

$$G(\xi_1, \dots, \xi_{nm}) = vMv^T, \quad v = (\xi_1, \dots, \xi_{nm}), \quad (5)$$

where M is an $nm \times nm$ matrix composed from the elements h_{ij}^{kl} . The $\mathbf{k} \cdot \mathbf{p}$ Hamiltonians in \mathbb{R}^n are a special case of (4). They are symmetric as a matrix PDO so the associated quadratic form G will have M with only real eigenvalues λ_i (e. g. 16).

Using these notations, the procedure of obtaining the ellipticity condition for H is reduced to the question about the sign of λ_i for the associated M . More precisely, the matrix differential operator H will be elliptic if and only if all eigenvalues of the corresponding Hermitian M will have the same sign^{48,49}.

In general, it is a challenging task to calculate the eigenvalues of M explicitly, even for Hamiltonians with

dimension as small as 3×3 , but this has proved to be possible⁴¹ for highly symmetric and sparse band structure Hamiltonians like H^{LK} and several others considered here.

Taking into account the fact that the sequence of eigenenergies of H_0 is semi-bounded from below, for an approximation H^{LK} we obtain

$$\lambda_i < 0, \quad i = 0, 1, \dots, nm. \quad (6)$$

Constraints (6) guarantee the ellipticity (in strong sense⁵⁰) of Hamiltonian H . The operator H possesses a self-adjoint extension in $D(H) \subset \mathcal{H}^{n+2}(\Omega)$, $n > 0$, provided that the boundary $\partial\Omega$ is sufficiently smooth, as we have assumed in the previous section. Then it can be extended to a Hermitian operator by a closure in the norm [p. 113, 49] or via the Lax-Milgram procedure⁴⁸. From the physical point of view the smoothness characteristics of $D(H)$ fulfil the natural assumption of quantum theory that the state of the system must be a continuous function of spatial variables even when some coefficients of H have finite jumps, as it is the case for heterostructures consisting of different materials^{10,47}.

The direct calculation by (5) for H^{LK} ($n = 3$, $m = 6$) leads us to the 18×18 matrix M^{LK} with the following distinct eigenvalues:

$$\begin{aligned} \lambda_1 &= -E(\gamma_1 + 4\gamma_2 + 6\gamma_3), & \lambda_2 &= E(3\gamma_3 - \gamma_1 - 4\gamma_2), \\ \lambda_3 &= E(2\gamma_2 - \gamma_1 + 3\gamma_3), & \lambda_4 &= E(2\gamma_2 - \gamma_1 - 3\gamma_3), \end{aligned} \quad (7)$$

where $\lambda_1, \lambda_2, \lambda_3, \lambda_4$ have the multiplicity 2, 4, 6 and 6, respectively, $E = \frac{\hbar^2}{2m_0}$ and $\gamma_1, \gamma_2, \gamma_3$ are the Luttinger material parameters mentioned above. By substituting (7) into (6), we receive the system of linear inequalities with respect to $\gamma_1, \gamma_2, \gamma_3$. They describe the feasibility region Λ_- in the space of ordered triplets $\gamma_1, \gamma_2, \gamma_3$. In this work we shall call a triplet of numbers a, b, c feasible if $(a, b, c) \in \Lambda_-$. More generally, we call a set of material parameters admissible if the Hamiltonian based on this set is an elliptic partial differential operator.

When $(\gamma_1, \gamma_2, \gamma_3) \in \Lambda_-$ the Hamiltonian H^{LK} is an elliptic PDO with the semi-bounded sequence of eigenvalues. One can use similar reasoning to obtain the corresponding inequalities for other common representations of H^{LK} like those through the parameters A, B, C^1 . Evidently, any solution of (6) for (7) would have a unique corresponding solution in the A, B, C notation¹⁹ (the aforementioned ellipticity analysis in full detail is presented in [41]). The region Λ_- comprises an unbounded pyramid in \mathbb{R}^3 (cf. Fig. 1) with the following rays as its edges:

$$\begin{aligned} l_1 &= (8t, t, -2t), & l_2 &= (2t, t, 0), \\ l_3 &= (3t, 0, t), & l_4 &= (4t, -t, 0), \end{aligned}$$

where $t \in [0, \infty)$, and the vertex is situated at the origin $\gamma_1 = \gamma_2 = \gamma_3 = 0$. The boundary of Λ_- and the edges l_1, l_2, l_3, l_4 are illustrated in FIG. 1.

To determine ellipticity of H^{LK} , we gathered in Table I the material parameters $\gamma_1, \gamma_2, \gamma_3$ for GaAs, AlAs, InAs,

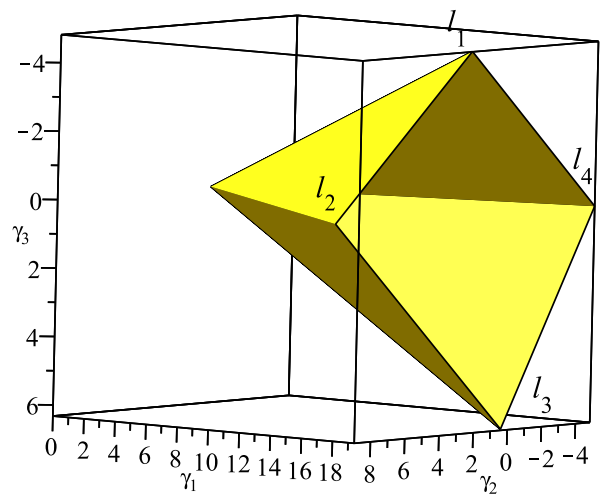


Figure 1. The part of the boundary of the feasibility region Λ_- along with the edges l_1, l_2, l_3, l_4 (color online).

GaP, AlP, InP, GaSb, AlSb, InSb, GaN, AlN, InN, C and evaluated $\lambda_1, \lambda_2, \lambda_3, \lambda_4$ for the gathered triplets. As it turned out, the eigenvalues $\lambda_1, \lambda_2, \lambda_4$ are negative for all analysed parameter sets. In that case the ellipticity is determined by the value λ_3 . We provide the values of λ_3/E along with two other parameter dependent quantities which are important for the current work's ellipticity analysis. The first is the distance d from the parameter triplet $(\gamma_1, \gamma_2, \gamma_3)$ to Λ_- . Second is an absolute ratio ρ between positive and negative values of $\lambda_1, \lambda_2, \lambda_3, \lambda_4$.

From Table I one can observe that among all analysed materials only carbon has admissible sets of parameters (the last two sets from of Table I indicated by 0 in the ρ column). All other gathered parameters yield $\lambda_3 > 0$. That is why the Hamiltonian H^{LK} is not elliptic for the corresponding materials. It may even have no symmetric domain $D(H^{LK})$ as opposed to the original partial differential operator H_0 . Moreover, instead of the inclusion $D(H^{LK}) = D(H) \subset D(H_0) \subset \mathcal{H}^3(\Omega)$ we have only

$$D(H^{LK}) = D(H) \subset \mathcal{H}^1(\Omega). \quad (8)$$

It means that the discontinuous solutions of (1) are theoretically possible. They will occur in the models with jump discontinuous coefficients⁵², which is the case for heterostructure materials. Additionally, the double degeneracy of $\lambda_3 > 0$ from (7) means that for certain Ω there exists a two-dimensional manifold of $D(H^{LK})$ with non-physical in terms of (8) solutions to (1). Thus, the momentum operator from (1), will be ill-defined for such eigenstates of H^{LK} (by the embedding theorems, [p. 119, 49]). All the above arguments allow us to conclude that the H^{LK} does not provide a sufficiently good approximation to H_0 , preserving the type of the PDO, for the most of available data.

Let us return to the feasible parameters from Table I. For carbon the parameter values were analyzed earlier⁵³

Table I. The material parameters for ZB type crystals, d – distance from the point $(\gamma_1, \gamma_2, \gamma_3)$ to the feasibility region Λ_-

#	El	γ_1	γ_2	γ_3	λ_3/E	d	ρ	#	El	γ_1	γ_2	γ_3	λ_3/E	d	ρ
1	GaAs ³⁰	6.980	2.060	2.930	5.930	1.585	0.117	23	InP ^{eh}	5.040	1.560	1.730	3.270	0.874	0.094
2	GaAs ^a	7.100	2.020	2.910	5.670	1.515	0.111	24	InP ³¹	6.280	2.085	2.755	6.156	1.645	0.129
3	GaAs ^b	7.800	2.460	3.300	7.020	1.876	0.121	25	GaSb ³⁰	13.400	4.700	6	14	3.742	0.134
4	GaAs ^c	6.950	2.250	2.860	6.130	1.638	0.119	26	GaSb ^{ag}	11.800	4.030	5.260	12.040	3.218	0.132
5	GaAs ^d	6.850	2.100	2.900	6.050	1.617	0.120	27	GaSb ^b	13.100	4.500	6	13.900	3.715	0.136
6	GaAs ^e	6.800	2.400	1	1	0.267	0.025	28	GaSb ²⁹	13.300	4.400	5.700	12.600	3.367	0.125
7	GaAs ^g	7.200	2.500	1.100	1.100	0.294	0.025	29	GaSb ³¹	11	3	4.368	8.105	2.166	0.105
8	GaAs ³¹	7.150	2.030	2.959	5.788	1.547	0.113	30	AlSb ³⁰	5.180	1.190	1.970	3.110	0.831	0.090
9	AlAs ³⁰	3.760	0.820	1.420	2.140	0.572	0.087	31	AlSb ²⁹	4.150	1.010	1.750	3.120	0.834	0.108
10	AlAs ²⁹	3.760	0.900	1.420	2.300	0.615	0.091	32	AlSb ³¹	4.120	1.045	1.715	3.115	0.832	0.108
11	AlAs ³¹	4.030	1.045	1.697	3.150	0.842	0.110	33	InSb ³⁰	34.800	15.500	16.500	45.700	12.214	0.154
12	InAs ³⁰	20	8.500	9.200	24.600	6.575	0.148	34	InSb ^a	36.130	16.240	17.340	48.370	12.927	0.156
13	InAs ²⁹	20.400	8.300	9.100	23.500	6.281	0.142	35	InSb ^b	36.410	15.940	16.990	46.440	12.412	0.151
14	InAs ²⁹	19.670	8.370	9.290	24.940	6.665	0.151	36	InSb ^c	35.080	15.640	16.910	46.930	12.543	0.156
15	InAs ³¹	19.700	8.400	9.280	24.939	6.665	0.151	37	InSb ³¹	35	15.700	16.821	46.864	12.525	0.156
16	GaP ³⁰	4.050	0.490	1.250	0.680	0.182	0.030	38	GaN ³⁰	2.670	0.750	1.100	2.130	0.569	0.111
17	GaP ^{agi}	4.200	0.980	1.660	2.740	0.732	0.096	39	GaN ²⁹	3.080	0.860	1.260	2.420	0.647	0.110
18	AIP ³⁰	3.350	0.710	1.230	1.760	0.470	0.081	40	GaN ⁵¹	5.050	0.600	1.787	1.511	0.404	0.051
19	AIP ^{agi}	3.470	0.060	1.150	0.100	0.027	0.006	41	AlN ³⁰	1.920	0.470	0.850	1.570	0.420	0.115
20	InP ³⁰	5.080	1.600	2.100	4.420	1.181	0.118	42	InN ^k	3.720	1.260	1.630	3.690	0.986	0.129
21	InP ^a	5.150	0.940	1.620	1.590	0.425	0.052	43	C ²⁹	2.540	-0.100	0.606	-0.922	0	0
22	InP ^{bg}	6.280	2.080	2.780	6.220	1.662	0.130	44	C ²⁹	3.610	0.090	1.101	-0.127	0	0

^a Set 1 from 29^b Set 2 from 29^c Set 3 from 29^d Set 4 from 29^e Set 5 from 29^f Set 6 from 29^g Obtained by extrapolation from 5-level model^h Measured at $T = 300K$ ⁱ Set from 31^k The sets from 30 29

and it was noted that they don't agree well with the Hall effect experimental measurements. In the earlier work¹⁹ we showed that experimentally consistent sets for C are not admissible in terms of ellipticity.

Concerning the rest of the materials from Table I we observe a clear correlation between the average distance to Λ_- per material and the size of the fundamental bandgap. Namely the sets for the large-bandgap materials: AIP, AlAs, GaP, GaN, InP are noticeably close ($d < 1$) to Λ_- . The closest in terms of the distance set number 19 for AIP can be made elliptic by the direct adjustment. Other materials have smaller gap and as a consequence are further away. The average distance to Λ_- for GaAs is around 1.7. For InAs the distance is more than 6. The indium antimonide is an extreme case here, having distance of more than 12. This material has the smallest bandgap and the high curvature of light-hole bands. It is known from the experiments^{2,54,55} that the valence-band-only Luttinger-Kohn model is insufficient for InSb like materials, and presented analysis support this fact theoretically. The ellipticity of the higher band $k \cdot p$ models are considered in the next sections.

IV. EIGHT-BAND HAMILTONIANS

This section is devoted to the analysis of Kane model^{33,36}. The basis set of 8×8 Kane Hamiltonian³³

contains two more elements $|S \uparrow\rangle$ and $|S \downarrow\rangle$ in addition to the basis set of H^{LK} . These new elements of basis represent the influence of the innermost conduction band. Recall that the influence of the out-of-basis states is again treated perturbatively up to the second order by using the Löwding perturbation theory. In this section we will follow the exposition of [33], because it presents the most general description of 8×8 Kane Hamiltonian for zinc blende crystals. Naturally, the results presented here remain valid⁵⁶ for other versions^{37,57,58} of the same Hamiltonian. Since our main focus is to check the ellipticity conditions we shall drop the spin-orbit interaction part, labelled as $H_{s.o.} + H'_{s.o.}$ in eq. (13) from [33]. This part of the Hamiltonian is linear in k and therefore won't affect the form of G . (as we have mentioned before, only second order terms in k are essential for ellipticity analysis) Then, following Kane³⁶, we rewrite the resulting operator in the block-diagonal form

$$H^K = \begin{pmatrix} H_{\uparrow}^K & 0 \\ 0 & H_{\downarrow}^K \end{pmatrix},$$

where H_{\uparrow}^K is the Kane 4×4 interaction matrix², given by (9) in the basis $|S \uparrow\rangle, |X \uparrow\rangle, |Y \uparrow\rangle, |Z \uparrow\rangle$ ³³. The matrix H_{\downarrow}^K that is also defined by (9), acts upon the spin-down part of the basis $|S \downarrow\rangle, |X \downarrow\rangle, |Y \downarrow\rangle, |Z \downarrow\rangle$.

$$H_{\uparrow}^K = \begin{pmatrix} E_c + (E + A') \mathbf{k}^2 & iP_0 k_x + Bk_y k_z & iP_0 k_y + Bk_x k_z & iP_0 k_z + Bk_x k_y \\ -iP_0 k_x + Bk_y k_z & E_v + M'(k_y^2 + k_z^2) + L'k_x^2 + E\mathbf{k}^2 & N'k_x k_y & N'k_x k_z \\ -iP_0 k_y + Bk_x k_z & N'k_x k_y & E_v + M'(k_y^2 + k_z^2) + L'k_x^2 + E\mathbf{k}^2 & N'k_y k_z \\ -iP_0 k_z + Bk_x k_y & N'k_x k_z & N'k_y k_z & E_v + M'(k_y^2 + k_z^2) + L'k_x^2 + E\mathbf{k}^2 \end{pmatrix}. \quad (9)$$

Parameters A', B, P_0, M', N', L' are known as Kane parameters³⁶, their definitions are provided in Table 4.2 of 37. The quantities E_c and E_v are the conduction- and valence-band energies correspondingly, E is equal to $\frac{\hbar^2}{2m_0}$, as before. The parameter A' represents the influence of the higher bands on the conduction band included into the basis. The parameter P_0 accounts for a mixing of conduction and valence band states away from $\mathbf{k} = \mathbf{0}$. B is a so-called inversion asymmetry parameter. It is equal to zero in the materials with centrosymmetric crystal structure like diamond³³. By setting $B = 0$ in (9) we obtain a simplified version of (9) that is known as Bir-Pikus 4×4 Hamiltonian. The general case of H_K when $B \neq 0$ was studied by T. Bahder (Eq. (15) in [33]). In practice the mentioned parameters are fitted to experimental data; It is frequently assumed in the literature that the simplified version of H_K provides a sufficiently good description of the physical phenomena in ZB crystals with face-centered lattice too. As we will later demonstrate, the Hamiltonian of such simplified model is non-elliptic for all studied material parameter sets and therefore is prone to the appearance of spurious solutions. The parameter B can not be set to zero for the materials where $E + A' < 0$.

Similarly to the 6×6 case, it is common to rewrite Hamiltonian H^K in the basis where its spin-orbit interaction part becomes diagonal. Usually one additionally pre-multiplies the original basis functions to make inter-band matrix elements and possibly other physically relevant quantities real-valued.

Direct calculation of eigenvalues for the quadratic form associated with H_{\uparrow}^K , described in details for the Luttinger–Kohn case from the previous section, gives us five distinct eigenvalues

$$\begin{aligned} \lambda'_1 &= E + L' + N', \\ \lambda'_2 &= E + L' - \frac{1}{2}N', \\ \lambda'_3 &= E + M' - \frac{1}{2}N', \\ \lambda'_4 &= E + \frac{2A' + 2M' + N'}{4} - \sqrt{\frac{(2A' - 2M' - N')^2}{16} + \frac{B^2}{2}}, \\ \lambda'_5 &= E + \frac{2A' + 2M' + N'}{4} + \sqrt{\frac{(2A' - 2M' - N')^2}{16} + \frac{B^2}{2}}. \end{aligned} \quad (10)$$

The presence of the second order conduction-valence band mixing, characterized by the parameter B of Kane Hamiltonian (9), is reflected in (10) by the pair of eigenvalues λ'_1, λ'_5 , which are both determined by the whole set

of the principal Hamiltonian parameters N, M, L, A', B . Note that, if one removes the mixing by setting $B = 0$, this property disappears and the eigenvalues λ'_4, λ'_5 are turned into

$$\lambda'_{04} = E + M' + \frac{1}{2}N', \quad \lambda'_{05} = E + A'.$$

A. Ellipticity analysis in the absence of inversion asymmetry

We analyze the set $\lambda'_1, \lambda'_2, \lambda'_3, \lambda'_{04}, \lambda'_{05}$ associated with $B = 0$ in H^K first. The fifth eigenvalue λ'_{05} in (10) is related to the conduction band of (9) because its corresponding three-dimensional eigenspace (λ'_{05} is triple degenerate) has only 3 first coordinates not equal to zero. Hence this eigenspace is orthogonal to the space associated with the valence bands. Those are characterized by the eigenvalues $\lambda'_1, \lambda'_2, \lambda'_3, \lambda'_{04}$ with degeneracy 1, 2, 3, 3, respectively. The following system of inequalities ensures ellipticity of 8×8 ZB Hamiltonian³³ with zero B

$$\begin{cases} E + L' + N' < 0 \\ E + L' - \frac{1}{2}N' < 0 \\ E + M' - \frac{1}{2}N' < 0 \\ E + M' + \frac{1}{2}N' < 0 \\ E + A' > 0. \end{cases} \quad (11)$$

As we mentioned, the eigenvalues $\lambda'_1, \lambda'_2, \lambda'_3, \lambda'_{04}$ are related to the valence band, hence the sign of the first four inequalities from (11) is the same as in (6). The opposite sign of the fifth inequality reflects its correspondence to the conduction band. Due to the electron-hole duality, the conduction band eigen-energies need to be semi-bounded from below. The presence summand E in system (11) is connected with the differences in the definition of Dresselhaus parameters⁵⁹ and L', M' ³³.

To compare the result for the 8×8 ZB Hamiltonian with the previously obtained results for the 6×6 Hamiltonian we define the dimensionless parameters $\gamma'_1, \gamma'_2, \gamma'_3$

similar to the Luttinger triplet^{37,54,57}

$$\begin{aligned}\gamma'_1 &= -\frac{1}{3}(L' + 2M')\frac{2m_0}{\hbar^2} - 1 \\ \gamma'_2 &= -\frac{1}{6}(L' - M')\frac{2m_0}{\hbar^2} \\ \gamma'_3 &= -\frac{1}{6}N'\frac{2m_0}{\hbar^2}.\end{aligned}$$

Hereby, the system (11) is transformed to

$$\begin{cases} -\gamma'_1 - 4\gamma'_2 - 6\gamma'_3 < 0 \\ -\gamma'_1 - 4\gamma'_2 + 3\gamma'_3 < 0 \\ -\gamma'_1 + 2\gamma'_2 + 3\gamma'_3 < 0 \\ -\gamma'_1 + 2\gamma'_2 - 3\gamma'_3 < 0 \\ 1 + A > 0, \end{cases} \quad (12)$$

with $A = A'/E$.

The modified and the original Luttinger parameters $\gamma_1, \gamma_2, \gamma_3$ are connected by the formulas⁵⁴

$$\gamma'_1 = \gamma_1 - \frac{E_p}{3E_g}, \quad \gamma'_2 = \gamma_2 - \frac{E_p}{6E_g}, \quad \gamma'_3 = \gamma_3 - \frac{E_p}{6E_g}, \quad (13)$$

where $E_p = P_0^2/E$, $E_g = E_c - E_v$ is a fundamental bandgap energy, P_0 is the Kane parameter from (9).

As it was expected, four out of five obtained inequalities (12), which represent the ellipticity constraints for the valence band part of H^K , have the structure equivalent to that for the LK Hamiltonian (7). Hence, the feasibility region of the valence-band part of H^K in the space of parameters $(\gamma'_1, \gamma'_2, \gamma'_3)$ coincides with the feasibility region Λ_- of H^{LK} , depicted in FIG. 1. It means that if $(\gamma'_1, \gamma'_2, \gamma'_3) \in \Lambda_-$, the valence-band part of the Hamiltonian H^K in the position representation is an elliptic partial differential operator. Then, the transformation given by (13) can be geometrically interpreted as a shift in the space of parameters proportional to vector $\mathbf{v}' = (-2, -1, -1)$. This shift reduces the value of λ'_3 and, as we shall soon see, brings the majority of the non-elliptic parameter triplets $(\gamma_1, \gamma_2, \gamma_3)$ closer to the feasibility region.

The dimensionless parameter A from the fifth inequality, that complements a set of ellipticity constraints (12), is responsible for a coupling between the conduction band and other states. It is commonly assumed that the in-basis valence bands are the major contributors to A . The value of A is determined by matching its value to the effective mass of conduction band m_c , determined experimentally using the formula

$$A = \frac{m_0}{m_c} - 1 - E_p \frac{E_g + \frac{2}{3}\Delta}{E_g(E_g + \Delta)}. \quad (14)$$

The magnitude of this parameter is clearly affected by the size of band-gap E_g and spin-splitting Δ . The experimental nature of m_c does not factor out other possible contributions to A . For that reason we extended the collection of parameter sets from Table I by those stemming from the same sets of Luttinger parameters and the

different values of bandgap energy E_g (measured within different experimental setups). We also added a parameter set obtained by fitting the bandstructure of 8×8 Hamiltonian to the bandstructure calculated by ab-initio methods⁵⁸. All the data pertaining to the ellipticity analysis of 8×8 Hamiltonian is collected in Table II. In each case the modified Luttinger parameters $\gamma'_1, \gamma'_2, \gamma'_3$ were calculated by using (13) and the values of P_0^2, E_g provided in the dataset source. For those sources from the table that have P_0^2 unavailable we use the values collected by I. Vurgaftman, J. R. Meyer and L. R. Ram-Mohan³⁰.

The ellipticity conditions of H^K are still violated for all materials presented in Table I. The situation is, however, more complex than for the 6×6 Hamiltonian. To illustrate that, we supplied in Table II the values of $\lambda'_1 - \lambda'_{05}$, the distance d to the feasibility region from $(\gamma'_1, \gamma'_2, \gamma'_3)$ and the measure of non-ellipticity ρ which is defined in the same way as for the 6×6 Hamiltonian case.

Overall, we can confirm the reduction of average distance to the feasibility region for all materials, especially for InAs and InSb. Furthermore, for several materials there exist parameter sets that are close to satisfy the full set of ellipticity constraints described by (12). Those are narrow gap semiconductor InSb (sets #37; #38 from Table II) and, perhaps more surprisingly, the materials with larger band-gap InP, AlAs and AlSb (sets #25, #10; #11, and #33). For these materials the corresponding parameter sets can be made elliptic by direct adjustment of $\gamma'_1, \gamma'_2, \gamma'_3, A$.

Certain parameter sets for AlP, AlSb and InAs satisfy ellipticity conditions for the valence band part of the Hamiltonian and do not satisfy the conduction-band constraint (inequality 5 from (12)). Among those, the sets #20, #33 for AlP, AlSb reported in [30] differ sharply in the size of γ_2 from two other sets for these materials collected in Table II. For AlP this can be explained by the fact that in the absence of direct experimental data most of the material parameters were extrapolated from measurements for ternary alloys and ab-initio calculations which carries a lot of uncertainty. The authors of [30] performed readjustment of the Luttinger parameters to better match the experimental photoluminescence results on AlP/GaP heterostructures⁶¹. The set #33 for AlSb is based on the available theoretical calculations from various sources and the simultaneous fitting of $\gamma_1, \gamma_2, \gamma_3$ to the experimentally-determined hole effective masses along [001], [110] and [111] directions³⁰.

For InAs we can judge from the size of $\lambda'_1 - \lambda'_{04}$ that the triplets $(\gamma'_1, \gamma'_2, \gamma'_3)$ of its parameter sets are right near the side of Λ_- described by $\lambda'_2 = 0$. Two are inside (sets #12; #13) and two others are slightly off (sets #14; #15). The values of λ'_{05} for all four parameter sets are grouped near the value $\lambda'_{05} = -4.8$ and thus the conduction part of the Hamiltonian is, again, far from being elliptic.

All material parameter sets for GaAs violate two out of four ellipticity conditions for the valence-band part, although one parameter set #3 from Table II stays close to Λ_- ($d = 0.34$). However, it violates the ellipticity con-

Table II. The material data for 8×8 ZB Hamiltonian with $B = 0$, d – distance from the point $(\gamma_1, \gamma_2, \gamma_3)$ to the feasibility region Λ_- . The positive values of $\lambda'_1/E - \lambda'_{05}/E$ are printed in bold.

#	El	E_p	E_g	Δ_{SO}	A'	γ'_1	γ_1	γ'_3	λ'_1/E	λ'_2/E	λ'_3/E	λ'_{04}/E	λ'_{05}/E	d	ρ	Δ_{05}^{\min}	Δ_{05}^{\max}
1	GaAs ³⁰	28.80	1.52	0.341	-3.88	0.66	-1.10	-0.23	5.12	3.05	-3.55	-2.17	-2.88	0.70	1.43	5.73	6.67
2	GaAs ^a	28.80	1.52	0.341	-3.88	0.78	-1.14	-0.25	5.28	3.03	-3.81	-2.31	-2.88	0.73	1.36	5.69	7.15
3	GaAs ^b	28.80	1.52	0.341	-3.88	1.48	-0.70	0.14	0.48	1.74	-2.46	-3.30	-2.88	0.34	0.39	3.27	4.62
4	GaAs ^c	28.80	1.52	0.341	-3.88	0.63	-0.91	-0.30	4.81	2.11	-3.35	-1.55	-2.88	0.66	1.41	3.96	6.29
5	GaAs ^e	28.80	1.52	0.341	-3.88	0.48	-0.76	-2.16	15.52	-3.92	-8.48	4.48	-2.88	2.13	1.61	8.41	15.92
6	GaAs ^g	28.80	1.52	0.341	-3.88	0.88	-0.66	-2.06	14.12	-4.42	-8.38	3.98	-2.88	1.94	1.41	7.47	15.74
7	GaAs ³¹	28.80	1.52	0.346	-3.86	0.83	-1.13	-0.20	4.89	3.09	-3.69	-2.49	-2.86	0.67	1.29	5.79	6.93
8	GaAs ⁵⁸	25.47	1.52	0.341	-3.34	1.28	-0.73	0.03	1.46	1.73	-2.65	-2.83	-2.34	0.34	0.58	3.25	4.98
9	AlAs ³⁰	21.10	3.10	0.280	-0.95	1.49	-0.31	0.29	-1.94	0.62	-1.26	-2.98	0.05	0.12	0.10	1.21	2.46
10	AlAs ²⁹	21.10	3.10	0.280	-0.95	1.49	-0.23	0.29	-2.26	0.30	-1.10	-2.82	0.05	0.06	0.05	0.59	2.15
11	AlAs ³¹	21.10	3.14	0.275	-0.87	1.79	-0.07	0.58	-4.95	0.24	-0.21	-3.67	0.13	0.05	0.03	0.47	0.41
12	InAs ³⁰	21.50	0.42	0.390	-5.79	2.81	-0.09	0.61	-6.08	-0.62	-1.18	-4.82	-4.79	-0.12	0	4.79	1.98
13	InAs ²⁹	21.50	0.42	0.390	-5.79	3.21	-0.29	0.51	-5.08	-0.52	-2.28	-5.32	-4.79	-0.10	0	4.79	3.82
14	InAs ^{bg}	21.50	0.42	0.390	-5.79	2.48	-0.22	0.70	-5.77	0.50	-0.84	-5.02	-4.79	0.10	0.04	4.79	1.41
15	InAs ³¹	21.50	0.42	0.380	-5.81	2.55	-0.17	0.71	-6.11	0.26	-0.78	-5.02	-4.81	0.05	0.02	4.81	1.31
16	GaP ³⁰	31.40	2.89	0.080	-4.09	0.42	-1.32	-0.56	8.25	3.18	-4.76	-1.38	-3.09	1.13	1.86	6.30	9.43
17	GaP ^{ag}	22.20	2.88	0.080	-0.95	1.63	-0.30	0.38	-2.66	0.71	-1.11	-3.37	0.05	0.14	0.10	1.42	2.21
18	GaP ^b	22.20	2.88	0.080	-0.95	1.48	-0.79	-0.03	1.91	1.59	-3.17	-2.97	0.05	0.31	0.57	3.16	6.29
19	GaP ³¹	31.40	2.90	0.080	-4.06	0.58	-0.82	-0.15	3.63	2.24	-2.69	-1.77	-3.06	0.50	1.32	4.45	5.34
20	AlP ³⁰	17.70	3.63	0.070	-1.30	1.72	-0.10	0.42	-3.82	-0.06	-0.68	-3.18	-0.30	-0.01	0	0.30	1.35
21	AlP ^{ag}	17.70	3.63	0.070	-1.30	1.84	-0.75	0.34	-0.86	2.18	-2.34	-4.36	-0.30	0.43	0.29	4.33	4.65
22	AlP ³¹	17.70	3.63	0.070	-1.30	1.84	-0.75	0.33	-0.85	2.14	-2.34	-4.34	-0.30	0.42	0.28	4.26	4.66
23	InP ³⁰	20.70	1.42	0.108	-2.62	0.23	-0.82	-0.32	5.00	2.09	-2.85	-0.91	-1.62	0.69	1.89	4.08	5.57
24	InP ^a	16.70	1.45	0.108	0.36	1.32	-0.97	-0.29	4.34	1.69	-4.15	-2.39	1.36	0.60	0.92	3.31	8.11
25	InP ^{bg}	20.40	1.56	0.108	-1.22	1.92	-0.10	0.60	-5.11	0.28	-0.32	-3.92	-0.22	0.06	0.03	0.55	0.63
26	InP ^{eh}	17.50	1.47	0.108	-0.09	1.06	-0.43	-0.26	2.23	-0.12	-2.70	-1.14	0.91	0.31	0.56	1.09	5.28
27	InP ³¹	20.70	1.34	0.108	-3.44	1.15	-0.48	0.19	-0.35	1.35	-1.54	-2.68	-2.44	0.26	0.29	2.63	3.01
28	GaSb ³⁰	27	0.81	0.760	-3.25	2.32	-0.84	0.46	-1.70	2.43	-2.63	-5.37	-2.25	0.48	0.25	4.07	4.40
29	GaSb ^{ag}	22.40	0.81	0.725	1.39	2.60	-0.57	0.66	-4.31	1.65	-1.75	-5.73	2.39	0.32	0.14	2.79	2.95
30	GaSb ^b	26.10	0.81	0.725	-2.45	2.39	-0.86	0.64	-2.81	2.97	-2.17	-6.03	-1.45	0.58	0.27	5.01	3.66
31	GaSb ²⁹	25	0.81	0.725	-1.31	3.04	-0.73	0.57	-3.52	1.59	-2.79	-6.21	-0.31	0.31	0.13	2.69	4.71
32	GaSb ³¹	27	0.75	0.756	-5.34	-1	-3	-1.63	22.79	8.11	-9.89	-0.11	-4.34	3.13	3.09	13.50	16.48
33	AlSb ³⁰	18.70	2.39	0.676	-1.12	2.57	-0.12	0.66	-6.09	-0.11	-0.81	-4.79	-0.12	-0.02	0	0.12	1.50
34	AlSb ²⁹	18.70	2.39	0.680	-1.12	1.54	-0.30	0.44	-3.02	0.98	-0.80	-3.46	-0.12	0.19	0.13	1.81	1.48
35	AlSb ³¹	18.70	2.30	0.673	-1.37	1.41	-0.31	0.36	-2.33	0.91	-0.95	-3.11	-0.37	0.18	0.14	1.68	1.76
36	InSb ³⁰	23.30	0.24	0.810	-0.46	1.75	-1.02	-0.02	2.50	2.27	-3.87	-3.73	0.54	0.45	0.63	3.37	5.75
37	InSb ^a	23.20	0.24	0.803	-0.13	3.25	-0.20	0.90	-7.85	0.25	-0.95	-6.35	0.87	0.05	0.02	0.37	1.41
38	InSb ^b	23.42	0.24	0.803	-0.37	3.44	-0.54	0.51	-4.31	0.25	-3.01	-6.05	0.63	0.05	0.02	0.37	4.47
39	InSb ^c	23.10	0.24	0.803	0.12	2.31	-0.74	0.53	-2.50	2.24	-2.22	-5.38	1.12	0.44	0.22	3.32	3.29
40	InSb ³¹	23.30	0.18	0.810	-21.07	-8.15	-5.87	-4.75	60.16	17.39	-17.86	10.66	-20.07	8.26	4.94	25.29	25.98
41	GaN ³⁰	25	3.30	0.017	-1.90	0.14	-0.51	-0.16	2.89	1.42	-1.66	-0.68	-0.90	0.40	1.84	2.83	3.31
42	GaN ⁶⁰	25	3.30	0.017	-1.90	0.17	-0.50	-0.15	2.76	1.38	-1.64	-0.72	-0.90	0.38	1.75	2.75	3.27
43	GaN ²⁹	25	3.30	0.017	-1.90	0.55	-0.40	-0.00	1.08	1.05	-1.37	-1.35	-0.90	0.21	0.78	2.09	2.73
44	GaN ⁵¹	25	3.44	0.017	-1.59	2.63	-0.61	0.58	-3.64	1.54	-2.12	-5.58	-0.59	0.30	0.14	3.08	4.24
45	GaN ³²	16.86	3.07	0.017	-1.30	0.68	-0.28	0.06	0.07	0.63	-1.05	-1.42	-0.30	0.12	0.28	1.25	2.09
46	AlN ³⁰	27.10	6	0.019	-1.51	0.41	-0.28	0.10	0.13	1.01	-0.69	-1.27	-0.51	0.20	0.58	2.01	1.38
47	AlN ⁶⁰	27.10	5.40	0.019	-2.01	0.25	-0.37	0.01	1.14	1.26	-0.94	-1.02	-1.01	0.25	1.12	2.52	1.88
48	AlN ³²	23.84	5.63	0.019	-2.07	0.04	-0.36	-0.13	2.15	1.01	-1.13	-0.37	-1.07	0.30	2.20	2.01	2.26
49	InN ³⁰	25	1.94	0.006	-5.54	-0.58	-0.89	-0.52	7.23	2.57	-2.75	0.35	-4.54	0.99	3.69	5.14	5.50
50	InN ⁶⁰	17.20	0.78	0.005	-8.72	-3.63	-2.42	-2.05	25.56	7.16	-7.34	4.94	-7.72	3.51	5.13	14.28	14.64
51	InN ³²	11.37	0.53	0.005	-3.87	-0.34	-0.77	-0.46	6.13	2.04	-2.56	0.17	-2.87	0.84	3.25	4.06	5.11

^a Set 1 from 29^b Set 2 from 29^c Set 3 from 29^d Set 4 from 29^e Set 5 from 29^f Set 6 from 29^g Obtained by extrapolation from 5-level model^h Measured at $T = 300K$

dition for the conduction-band part by the same margin of approximately -2.9 as do other sets of GaAs parameters, let alone set #8 where the margin is slightly lower: $\lambda'_{05} \approx -2.34$. The indicated reduction of margin should be attributed to the optimization procedure⁵⁸ used to acquire set #8. As far as the ellipticity is concerned, this optimization procedure is no more effective than other acquisition methods.

The sets for GaN and AlN are failing first two valence-part constraints from (12) just like the most of the other material parameters. One exception is the set number 44 for GaN⁵¹, where the spherical symmetry of the heavy-hole and the light-hole bands is assumed. This assumption leads to the larger values of γ_1, γ_3 and smaller γ_2 ; and, as a consequence, more than five times smaller ratio ρ between positive and negative eigenvalues.

Even a more severe situation is observed for InN. The conduction-band eigenvalue λ'_{05} is noticeably below zero for all three available datasets ($\lambda'_{05} \approx -4.54; -7.72; -2.87$ for sets #49; #50; #51 accordingly). In addition, three out of four valence-band conditions are violated. It is important to highlight that the recently obtained set of parameters #51 features roughly two times larger values of γ_1, γ_2 and γ_3 and noticeably smaller E_p, E_g than two other sets #49, #50 reported earlier^{30,60}. As demonstrated in [32] set #51 recovers bandstructure better than two others sets for InN, discussed above. In terms of ellipticity, this set results in a lower, than others, distance to Λ_- ($d \approx 0.84$) and lower $\lambda'_{05} \approx 0.17$.

For GaP and GaSb the data seem inconclusive as the size and the sign of eigenvalues (10) are dependant on the choice the material parameter dataset. Sets #17, #29 from Landolt-Börnstein²⁹, based on the earlier data of P. Lawaetz²⁸, are most favourable in terms of ellipticity: $d \approx 0.14$, $\lambda'_{05} \approx 0.05$ for GaP; $d \approx 0.32$, $\lambda'_{05} \approx 2.39$ for GaSb. As a summary of the above analysis, we visualize in FIG. 2 the values of λ'_{05}, d for the selected parameter sets with the material-wise minimal distance to Λ_- . In this figure the ellipticity of Hamiltonian is depicted by the region (shaded in gray) where $\lambda'_{05} > 0$ and $d < 0$ simultaneously.

It is worth noticing that roughly 76% of parameter sets for analyzed materials fail the conduction-band constraint $\lambda'_{05} > 0$. This group includes all datasets for GaAs, InAs, AlP, AlSb, GaN, AlN, InN, quite important for applications. The positive (negative) sign of λ'_{05} is responsible for positive(negative) gain in the energy as we go from one conduction-band eigenvalue of Hamiltonian to the next in the position representation. In the momentum representation, the eigenvalue's sign and its magnitude is responsible for upward (downward) curvature of conduction band. In addition to the highlighted in section III issues caused by the non-ellipticity of valence-band part of the Hamiltonian H^K , the violation of condition $\lambda'_{05} > 0$ entails the existence of conduction-band related eigenstates of H^K with energies in the band-gap or the regions related to valence bands^{14,16,17,57}. This obviously poses a serious problem in applications.

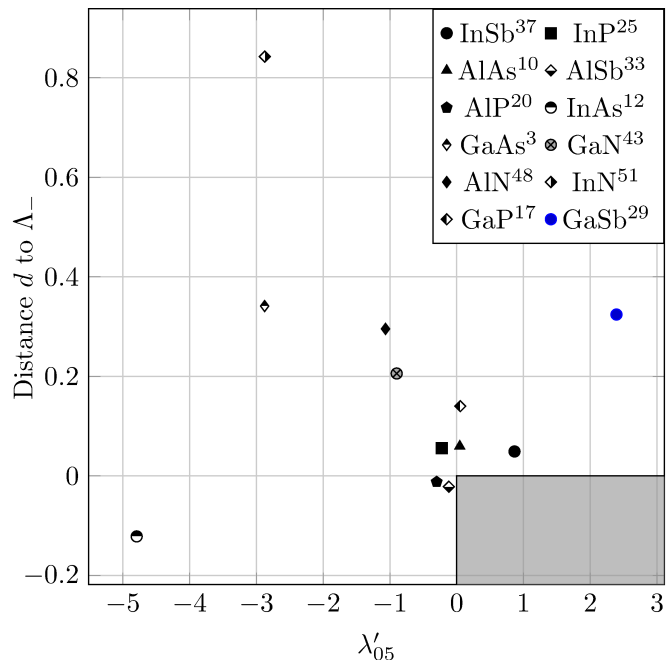


Figure 2. The values of quantities λ'_{05}, d for the list of selected material parameter sets from Table II (color online). The shaded region indicates pairs (λ'_{05}, d) based on the ellipticity parameters of 8×8 model³³

A rescaling procedure was introduced by B. Foreman in [20] (see also the work of S. Birner [57]) and has been adopted^{62,63} ever since as a way to make λ'_{05} positive and avoid the above-described type of spurious solutions. The idea of the procedure is to adjust the momentum matrix element E_p so that λ'_{05} is no longer negative. Let us assume that we target some value of $\lambda'_{05} = a$. Then, by using the definition of λ'_{05} and (14), we obtain⁵⁷

$$E_p = \left(\frac{m_0}{m_c} - a \right) \frac{E_g(E_g + \Delta_{SO})}{E_g + \frac{2}{3}\Delta_{SO}}. \quad (15)$$

Two values $a = 0$ and $a = 1$ are considered in the literature as a target for rescaling. The new value of E_p will necessarily affect the values of modified Luttinger parameters $\gamma'_1, \gamma'_2, \gamma'_3$ which are defined by (13). To figure out how this procedure would impact the ellipticity of the entire 8×8 ZB Hamiltonian H^K one needs to rewrite eigenvalues $\lambda'_1 - \lambda'_{04}$ as functions of E_p, E_g :

$$\lambda'_1 = \lambda_1 + 2E \frac{E_p}{E_g}, \quad \lambda'_{2/04} = \lambda_{2/4} + \frac{E}{2} \frac{E_p}{E_g}, \quad \lambda'_3 = \lambda_3 - \frac{E}{2} \frac{E_p}{E_g}.$$

By combining the above representations with (15) we obtain a new version of ellipticity constraints (12) for the valence-band part of H^K

$$\begin{aligned} \lambda_1 + 2E_m - \frac{2a}{E_r} < 0, & \quad \lambda_2 + \frac{1}{2}E_m - \frac{a}{2E_r} < 0, \\ \lambda_3 - \frac{1}{2}E_m + \frac{a}{2E_r} < 0, & \quad \lambda_4 + \frac{1}{2}E_m - \frac{a}{2E_r} < 0, \end{aligned} \quad (16)$$

where $E_m = \frac{m_0}{m_c E_r}$, $E_r = \frac{E_g + \frac{2}{3}\Delta_{SO}}{E(E_g + \Delta_{SO})}$ are two material-dependent constants. Now we substitute back $a = \lambda'_{05} + \Delta_{05}$ and solve system of inequalities (16) with respect to Δ_{05} . As a result, it will give us the range for the values of the rescaling parameter Δ_{05} that make the valence-band part of Kane Hamiltonian elliptic

$$E_r \max \left\{ \frac{1}{2}\lambda'_1, 2\lambda'_2, 2\lambda'_{04} \right\} < \Delta_{05} < -2\lambda'_3 E_r. \quad (17)$$

The calculated values for the ranges from (17) are provided in the last two columns of Table II. If $-\lambda'_{05} < -2\lambda'_3 E_r$, then the Hamiltonian can be made elliptic by setting Δ_{05} to the arbitrary value within range (17) so that $\lambda'_{05} + \Delta_{05}$ is positive. In practice one would also like to make sure that the numerical inaccuracies introduced by the eigenvalue calculation procedure for H^K will not overturn any of the signs of $\lambda'_1 - \lambda'_{05}$. To minimize that possibility and to keep Δ_{05} reasonably small we suggest the following formula for the selection of Δ_{05}

$$\Delta_{05} = \begin{cases} 2\Delta_m + 0.1, & \Delta_m + \lambda'_3 E_r < -0.1, \\ \Delta_m - \lambda'_3 E_r, & \text{otherwise.} \end{cases} \quad (18)$$

with $\Delta_m = \max \left\{ \frac{1}{4}\lambda'_1 E_r, \lambda'_2 E_r, \lambda'_{04} E_r, -\frac{\lambda'_{05}}{2E} \right\}$.

We carried out the rescaling procedure for the material parameters from Table II and selected the sets with minimal Δ_{05} for every given material. The resulting values of readjusted E_p , A' along with new values of modified Luttinger parameters are presented in Table III. It is also worth noting that the resulting value of $1 + A$ in our case is never equal to zero or one, as it was usually assumed by authors before^{20,57}. For many materials the value of adjusted parameter A is greater than 0.

To see the impact of rescaling on the band dispersion, in Table III we also supplied a maximum absolute difference (adjustment error) between the corresponding bands of bandstructure calculated over the 20% of three high symmetry paths ΓL , ΓK and ΓX pertaining to the first Brillouin zone (FBZ). Such a size of the domain for comparison is common³⁰ and motivated by the existing evidence⁵⁸ that the accurate fit of the $k \cdot p$ bandstructure to the state-of-the-art ab-initio calculations is possible over this part of FBZ. To ascertain the band that contributes most to the error we supplied in FIG. 3 a), and FIG. 4 the graphical comparison of band-structure diagrams for every set from Table III and the original sets of material parameters from Table II, on which they are based. For clarity, only bands with even numbers in the representation of 8×8 Hamiltonian³³ are plotted in these figures.

As one immediately notices from the last column of Table III, the chosen sets for AlN, AlP, AlSb, and AlAs materials are least susceptible to the performed rescaling procedure. The differences between the bandstructure for modified parameters sets (four topmost rows from

Table III. Selected material parameters, rescaled via (18) together with the difference between corresponding bands of 8×8 Hamiltonian³³ for original and rescaled parameters

El ^a	Δ_{05} ^b	E_p	A'	γ'_1	γ'_2	γ'_3	λ_v ^c	err ^d
AlN ⁴⁸	2.11	11.92	0.049	0.744	-0.004	0.226	-0.05	2.78
AlP ²⁰	0.40	16.24	-0.900	1.859	-0.036	0.484	-0.26	4.29
AlSb ³³	0.22	18.14	-0.900	2.646	-0.077	0.703	-0.23	5.84
AlAs ¹⁰	0.69	18.90	-0.262	1.728	-0.116	0.404	-0.05	9.35
GaN ⁴³	2.19	17.75	0.296	1.287	-0.037	0.363	-0.05	11.58
InP ²⁵	0.59	19.46	-0.632	2.120	0	0.700	-0.02	11.69
GaP ¹⁷	1.52	17.80	0.569	2.140	-0.050	0.630	-0.05	23.34
InSb ³⁷	0.47	23.05	0.336	3.462	-0.094	1.006	-0.07	32.66
InN ⁵¹	4.16	9.16	0.285	1.054	-0.071	0.240	-0.05	35.03
GaAs ³	3.37	23.35	-0.509	2.676	-0.102	0.738	-0.05	50.62
GaSb ²⁹	2.87	19.63	4.263	3.740	0	1.230	-0.05	171.40

^a Refer to the original dataset number from Table II

^b The quantity Δ_{05} describes the size of adjustment to A'

^c The values of λ_v are calculated via $\lambda_v = \max\{\lambda'_1, \lambda'_2, \lambda'_3, \lambda'_{04}\}$

^d Maximum difference in meV between the bandstructure for the original parameters from Table II and the rescaled parameters calculated by using (18) over the 20 % of the paths ΓL , ΓK and ΓX

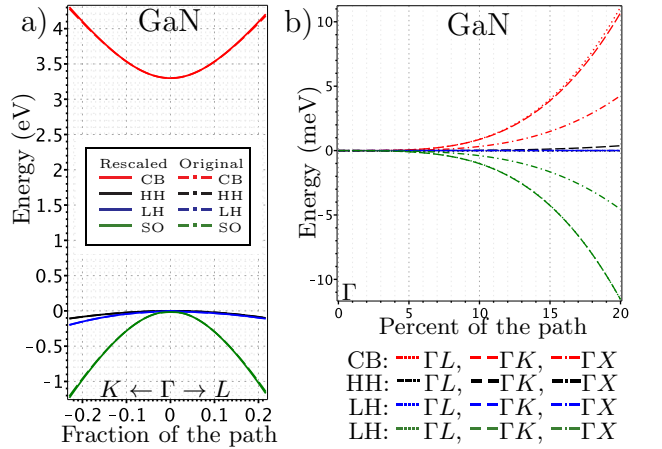


Figure 3. Comparison of original and rescaled parameter sets for GaN (color online): Conduction band (CB), heavy-hole (HL), light-hole (LH) and the split-off band (SO). a) Band-structure along the fraction of symmetry path $K - \Gamma - L$: original set 43 (solid), rescaled set from Table III (dashed); b) bandstructure adjustment error along the paths ΓL , ΓK and ΓX

Table III) and the original sets for materials from this group are less than 10 meV. We will call these differences bandstructure adjustment errors or simply errors, when it is unambiguous. For GaN and InP the errors of approximately 11 meV are also visually indistinguishable in FIG. 3 a) and FIG. 4. Thus we supplied in FIG. 3 b) their plot for GaN, that has an appropriate vertical scaling. This plot, typical for all analyzed materials except of InN, shows the behaviour of bandstructure adjustment error along three main paths ΓL , ΓK and ΓX . For the GaN, the errors along directions ΓL , ΓK are about 11

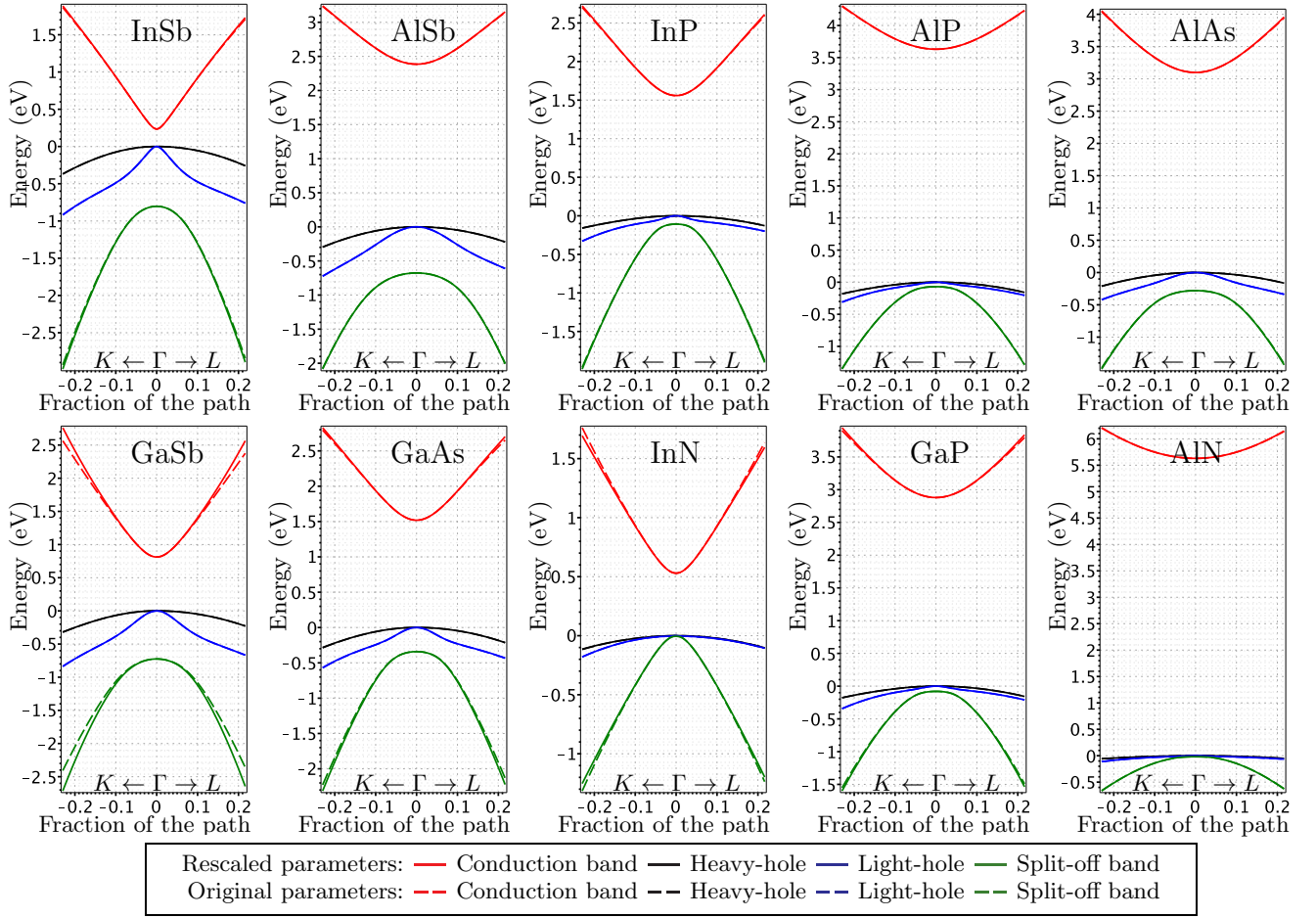


Figure 4. Comparison of bandstructure for the selected original parameter sets from Table II and the rescaled sets from Table III (color online). The band dispersion is plotted from even eigenenergies of 8×8 Hamiltonian³³ along the fraction of symmetry path $K - \Gamma - L$ in the vicinity of Γ : original sets (solid line), rescaled sets (dashed line).

meV, while the band errors in the direction ΓX is around two times lower. What makes this material unique is the fact that such tiny errors are the result of a significant change in the values of material parameters during the rescaling. Namely, the difference in E_p is around 29% and above 100% for γ'_1, γ'_2 .

The situation is more close to the anticipated for another group of materials: GaP, InN, GaAs. The relative differences in $E_p \approx 19\%$ for all three materials, but the error is higher for GaAs than for GaP and InP: 50.62 meV vs 23.34 meV and 35.02 meV, respectively. This can be explained by a closer proximity of p -like conduction bands in GaAs, that are treated perturbatively in the current model. For indium antimonide the band adjustment error of 32.66 meV (barely visible as a slightly higher curvature of conduction and SO bands in the first plot of FIG. 4) lays within the same range as for GaP, InN, GaAs. What is unusual is that these differences in band dispersion were produced by the smallest (among all analyzed materials) adjustment of $E_p - 0.6\%$, which resulted in only approximately 10% increase of γ'_1, γ'_3 . Such error sensitivity might be attributed to the very

small bandgap (see FIG. 4). The conduction band (CB) adjustment error for InSb is equal to 10.87 meV. That is about 3 times smaller than the valence band adjustment error and therefore invisible in the plot. The same is true for heavy hole and light hole bands.

Similar tendencies are valid for other materials from Table III. The performed adjustment of A leads to a slightly noticeable change in the conduction band dispersion. Heavy hole (HH) and light hole (LH) bands remain visually unaffected even though the differences are non-zero. The rescaling also causes an increase in the curvature of the split-off (SO) band, making it the main source of total valence-band adjustment error.

The maximum adjustment error of 171.4 meV was observed in gallium antimonide. We postpone a detailed discussion of GaSb till the next subsection and focus now on the following question: How the dispersion of CB and SO band can be corrected without braking ellipticity of the H^K Hamiltonian?

B. Ellipticity analysis for 8×8 ZB Hamiltonian with inversion-asymmetry present

To answer the question posed at the end of previous subsection, we will consider here the ellipticity conditions for the case of non-zero B in (9). In this case the ellipticity region in the parameter space $A', B, \gamma'_1, \gamma'_2, \gamma'_3$ is described by the system of inequalities

$$\begin{cases} \max \{-4\gamma'_2 - 6\gamma'_3, 3\gamma'_3 - 4\gamma'_2, 3\gamma'_3 + 2\gamma'_2\} < \gamma'_1 \\ E + A' + \lambda'_{04} - \sqrt{(E + A' - \lambda'_{04})^2 + 2B^2} < 0 \\ E + A' + \lambda'_{04} + \sqrt{(E + A' - \lambda'_{04})^2 + 2B^2} > 0. \end{cases} \quad (19)$$

The first inequality is just a compact form of inequalities 1-3 from (12), the value of λ'_{04} is equal to the one defined above, but written in a new parameter notation $\lambda'_{04} = -\gamma'_1 + 2\gamma'_2 - 3\gamma'_3$.

Despite a more complicated structure than in the situation with zero B , discussed earlier, one out of two B -dependent constrains in (19) is always fulfilled. To be more specific: if $E + A' \geq -\lambda'_{04}$ the third inequality from (19) is redundant, else, the second one is redundant. In each case, the remaining non-redundant inequality leads to the following constraint on B^2

$$B^2 - 2E^2(1 + A)(-\gamma'_1 + 2\gamma'_2 - 3\gamma'_3) > 0. \quad (20)$$

The combination of (20) with the first inequality from (19) yields a system of ellipticity constraints for 8×8 ZB Hamiltonian³³ with non-zero B

$$\begin{cases} \max \{-4\gamma'_2 - 6\gamma'_3, 3\gamma'_3 - 4\gamma'_2, 3\gamma'_3 + 2\gamma'_2\} < \gamma'_1 \\ 2E^2(1 + A)(-\gamma'_1 + 2\gamma'_2 - 3\gamma'_3) < B^2. \end{cases} \quad (21)$$

Inequality (20) is fulfilled for any B , when the parameter set $A, \gamma'_1, \gamma'_2, \gamma'_3$ satisfies conditions 4-5 from (12). Consequently, the admissible, in terms of (12), material parameters with zero B remain admissible even after the value of B is set to some nonzero number. In other words, B can be treated as an additional fitting parameter to be used in the subsequent adjustment step after the rescaling procedure is performed, but the additional ellipticity preserving readjustment of bandstructure is needed. We are especially interested in correcting the improper dispersion of the CB and SO bands, since it is a major source of errors (see Table III) for most of the rescaled material parameter sets.

Conducted numerical experiments⁵⁶ with different values of B indicate that the increase in $|B|$ leads to the increase in the curvature of conduction and SO bands along ΓK , ΓL and ΓX directions. For InN, that makes the CB adjustment error along those directions smaller at the expense of larger difference in SO band dispersion between the original set and the rescaled parameter set with non-zero B . The indicated behaviour of error and the fact that the error's dominating contribution comes

from CB and SO bands (see FIG. 3 b) mean that there exists an optimal value B that minimizes the error for chosen energy bands. For small errors and $B > 0$ the indicated behaviour is also influenced by the spin-splitting of bands away from Γ . Error can not be minimized for GaSb material, because the rescaled parameters with $B = 0$ already yield visibly higher curvature of CB than the original parameters (see GaSb plot in FIG. 4). We performed the error minimization by adjusting B for each selected parameter set from Table III and confirm that for all materials, except of InN, increase in $|B|$ makes error larger.

The first larger value of $|B| = 15.006$ for InN is a result of the error minimization over two conduction bands only. The conduction band error $\text{err}_{\text{CB}} = 8.352$ meV signifies that the correct dispersion of CB can be recovered almost perfectly by selecting the appropriate $|B|$. These stated differences between the obtained dispersion and the one for original parameter sets are caused by the non-zero spin-splitting of the CB states for $B \neq 0$, which is also witnessed experimentally^{64,65}. To illustrate the effects of spin-splitting and visualize the behaviour of adjustment error, we provide in FIG. 5 bandstructure plots for InN along selected directions together with the plot of direction-wise maximal absolute error between the banstructure of original set #51 from Table II with $B = 0$ and rescaled set from Table III with $B = 15.006$.

Notice from FIG. 5 b),c) that the spin-splitting is even more evident for LH and SO valence bands than for the conduction band depicted in FIG. 5 a). Direction-wise the magnitude of CB spin-orbit splitting depends on the ratio of the individual momentum components k_x/k_y , k_x/k_z , k_y/k_z . It is non-zero if all these ratios are not zero, infinity or one.

The overall eight-bands' adjustment error $\text{err} = 9.839$ meV is still more three times smaller for the calculated B than for $B = 0$ (green dotted and dash-dotted lines vs red solid line in FIG. 5 d). Now this error is dominated by the error of SO band that comes from dispersion along ΓK direction (FIG. 5 b). This kind of dominance is typical for the consider materials.

Starting from the same sets of parameters in Table III, we performed another optimization procedure with the aim of verifying at what extent the overall eight-bands' adjustment error can be minimized with help of B . The resulting value of $B = 14.805$ and error $\text{err} = 9.057$ meV are non-significantly differ from the results of the previous optimization procedure. The corresponding band dispersion for InN is visualized in FIG. 6 by using the layout of the previous figure.

The obtained minimal error is around 10 % smaller than the eight-bands' error of the previous optimization procedure and almost 6 times smaller than the banstructure error of rescaled parameters with zero B (see the last column of Table III).

For InN, the same conclusion can be made from FIG. 6 d), where the band-wise error dispersion (dotted and dash-dotted lines) is plotted along with the error dispersion of the elliptic parameter set with $B = 0$. The overall

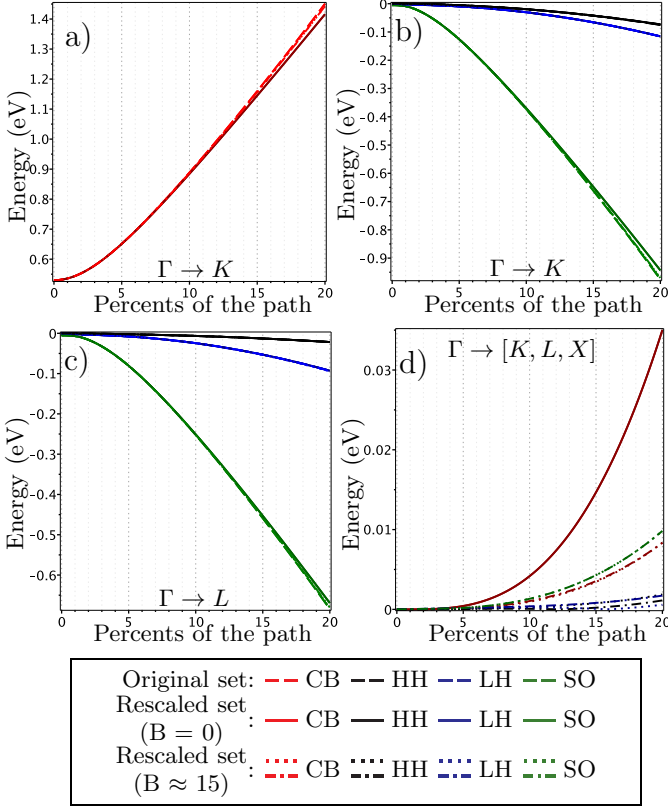


Figure 5. Comparison of original and rescaled parameter sets for InN (color online): original set #43 (solid); rescaled set from Table III with $B = 0$ (dashed) and with optimal $B = 15.006$ (dotted and dash-dotted). Bandstructure along the fraction of symmetry paths: a) Conduction band (CB) along ΓK ; b) Valence bands along ΓK ; c) Valence bands along ΓL ; d) Maximum absolute difference (direction-wise) between original and rescaled sets

error is apparently dominated by the adjustment error of CB and SO bands (FIG. 6 a,b). The errors of other bands are below 1 meV.

The error plots of FIG. 5 and FIG. 6 are also useful to quantify the magnitude of spin-splitting in CB, LH and SO bands for $B = 15.006$ and $B = 14.805$. The comparison of calculated spin-splitting parameters for GaAs and AlAs from Table III and the experimental values for CB along $(1, 1, 0)$ direction suggests that the value of B around 70-80 eV is needed for the 8×8 model to reach the reported experimental values⁶⁶⁻⁶⁸. For such B we observed the deviation in band dispersion of around 0.35-0.5 eV from the dispersion for zero B . Thus, spin-splitting errors are more dominant than the adjustment errors for selected material sets and possibly others (for the experimental values of B see Table 5.5 from [21] and the references therein). In order to achieve better accuracy with $B \neq 0$ one should use the bandstructure diagram with realistic spin-splitting of bands as an optimization target. Having that in hands, one can possibly get better results by applying the implemented two-step adjustment

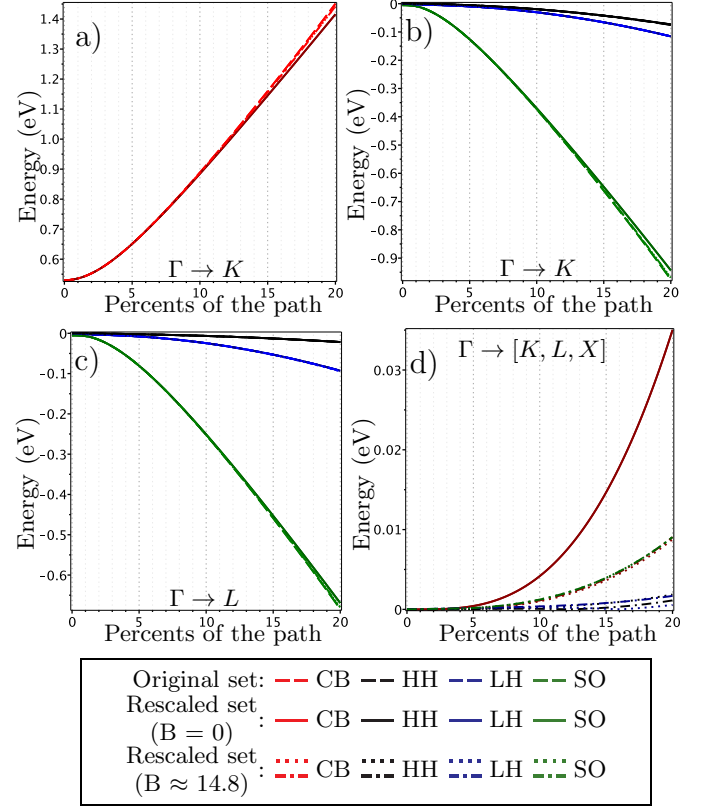


Figure 6. Comparison of original and rescaled parameter sets for InN (color online): original set #43 (solid); rescaled set from Table III with $B = 0$ (dashed) and with optimal $B = 14.805$ (dotted and dash-dotted). Bandstructure along the fraction of symmetry paths: a) Conduction band (CB) along ΓK ; b) Valence bands along ΓK ; c) Valence bands along ΓL ; d) Maximum absolute difference (direction-wise) between original and rescaled sets

procedure to other materials data entries from Table II where the range $(\Delta_{05}^{\min}, \Delta_{05}^{\max})$ for the adjustment parameter Δ_{05} is non-empty.

To clarify the use of $|B|$ in the above calculations we note, that similarly to ellipticity constraints (21), the sign of B^{55} has no effect on the eigenvalues of the Hamiltonian in momentum or position representation. It, however, affects the eigenstates of the Hamiltonian in both representations and therefore must be taken into consideration for experiments^{69,70} that make use of the eigenstates.

One can further increase the accuracy of admissible parameter set of 8×8 Hamiltonian by fitting⁵⁸ the full set of $A, \gamma'_1, \gamma'_2, \gamma'_3, B$ and using inequalities (21) as constraints for the fitting method. Our initial results in that direction show that this is possible for a wide range of materials. Besides, the adjustment with B alone is not a universal substitute for the optimally fitted parameter set $A, \gamma'_1, \gamma'_2, \gamma'_3, B$ because the effect of B on the bandstructure disappears if two out of three momentum components are zero.

Now, let us get back to ellipticity conditions (21). So

far we used B as a bandstructure fitting parameter, after the ellipticity of parameter set was established by rescaling procedure (13), (15), (18) with zero B . The procedure with adjustment of B can be used directly for the materials with the elliptic valence band part (e.g. sets #12, #13, #20, #33). For such materials we can overturn the negative sign of λ_5' and make the Hamiltonian fully elliptic by setting B to the appropriate (in terms of (20)) nonzero value. This allows to bypass the rescaling procedure altogether, which might be favourable in the light of its phenomenological nature. Another, more physically convenient, way to increase the accuracy of $k \cdot p$ Hamiltonian is to extend its basis set by adding new energy band states. The resulting Hamiltonians are analyzed in the next section.

To conclude the discussion on the ellipticity of 8×8 ZB Hamiltonians we apply the direct adjustment of B to several material parameter sets from Table II; namely sets #12, #13 for InAs, set #20 for AlP and set #33 for AlSb. Only those listed parameter sets yield elliptic valence band part of the Hamiltonian, i.e. the corresponding distance $d = 0$ in Table II. Notably, for each of the three materials the first listed set was reported in [30] – the work that is highly regarded as a source of overall physically consistent material parameters. For InAs, the direct adjustment of B is the only option to obtain the admissible parameter sets based on the data from Table II, because the admissible range $(\Delta_{05}^{\min}, \Delta_{05}^{\max}) \ni \Delta_{05}$ is empty for all its four table entries. For each above mentioned parameter sets we performed bandstructure error minimization procedure over the interval $|B| \in (|B|_{\min}, \infty)$ and reported the resulting value $|B|$, along with the errors in Table IV. Here $|B|_{\min}$ is the minimal solution of (20), with 0.1 substituted in place of 0 in the right-hand side to accommodate for possible numerical errors.

Table IV. Results of direct bandstructure error minimization procedures based on the adjustment of B .

El ^a	$ B _{\min}$	$ B ^b$	err ^c	err _{CB} ^d	err _{HH} ^d	err _{LH} ^d	err _{SO} ^d
InAs ¹²	25.90	25.90	0.073	0.073	0.013	0.061	0.073
InAs ¹³	27.21	27.21	0.081	0.077	0.013	0.064	0.081
AlP ²⁰	5.27	5.27	0.003	0.002	0.001	0.002	0.003
AlSb ³³	4.06	4.06	0.012	0.003	0.002	0.012	0.008

^a Refer to the original dataset number from Table II

^b B that minimizes the banstructure error

^c The minimal value of the error in eV calculated for the eight bands with a given B over 20 % of the paths ΓL , ΓK and ΓX

^d The errors err_{CB}, err_{HH}, err_{LH}, err_{SO} (all in eV) of conduction bands, heavy holes, light holes and split-off bands accordingly

For brevity we do not provide bandstructure or error plots based on the data from Table IV. Alternatively, we supplied the errors of CB, HH, LH, SO bands as separate entries in the table. For InAs and AlP the introduced bandstructure error is dominated by the differences in CB, SO and LH bands. The situation is different for AlSb for which the main contribution to the error comes from LH bands.

The results reported in Table IV clearly indicate that set #20 for AlP along with $B = 5.272$ lead to the smaller bandstructure adjustment error than the same-material set reported in Table III with $B = 0$. We recommend this for simulations based on the 8×8 ZB Hamiltonian³³ in the position representation. For InAs we suggest using the set 12 with $B = 25.898$. The set obtained as a result of two step optimization, reported above, is the most optimal for InN. For the rest of materials analyzed in this work we recommend the sets from Table III.

V. ELLIPTICITY OF 14×14 BAND MODELS

In this section we focus our attention on the ellipticity of two 14×14 ZB Hamiltonians that are frequently used in the literature^{34,42,71–79}. These two models are based on the extended basis set: six p -like valence band states and two s -like conduction states comprising the basis of 8×8 Hamiltonian studied in the previous section, plus six additional p -like conduction band states. They are introduced to better describe anisotropy of conduction band in the materials like GaAs, InP, InSb, where it is evidenced experimentally^{34,71,73,74}.

The first Hamiltonian proposed by W. Zawadzki, P. Pfeffer and H. Sigg in [72] and then extended^{34,74} to account for the influence of the out-of-basis bands perturbatively. We base our analysis on this later extended version described by equation (5) from [34]. The calculated⁵⁶ eigenvalues $\lambda_1'' - \lambda_5''$ of the quadratic form associated with this 14×14 ZB Hamiltonian are as follows

$$\begin{aligned}
 \lambda_1'' &= E(-\gamma_1'' - 4\gamma_2'' - 6\gamma_3'') \\
 \lambda_2'' &= E(-\gamma_1'' - 4\gamma_2'' + 3\gamma_3'') \\
 \lambda_3'' &= E(-\gamma_1'' + 2\gamma_2'' + 3\gamma_3'') \\
 \lambda_4'' &= E(-\gamma_1'' + 2\gamma_2'' - 3\gamma_3'') \\
 \lambda_5'' &= E.
 \end{aligned} \tag{22}$$

The CB part of the Hamiltonian is elliptic by design, since $\lambda_5'' > 0$ independently of materials parameters. The ellipticity of the valence-band part is guaranteed when $\lambda_1'' - \lambda_4''$ are all negative simultaneously. So in the end, we are getting exactly the same ellipticity conditions as for the 6×6 ZB Hamiltonian, albeit with the different Luttinger-like parameters (compare the above $\lambda_1'' - \lambda_4''$ with $\lambda_1' - \lambda_4'$ from (7)). These new Luttinger-like parameters $\gamma_1'', \gamma_2'', \gamma_3''$ can be obtained from the conventional Luttinger parameters by subtracting from $\gamma_1, \gamma_2, \gamma_3$ the contributions of p -like CB bands, that are no longer treated perturbatively. More precisely,

$$\begin{aligned}
 \gamma_1'' &= \gamma_1' - \frac{Q^2}{3EE_0'} - \frac{Q^2}{3E(E_0' + \Delta_0')}, \\
 \gamma_2'' &= \gamma_2' + \frac{Q^2}{6EE_0'}, \quad \gamma_3'' = \gamma_3' - \frac{Q^2}{6EE_0'}.
 \end{aligned} \tag{23}$$

Here E_0 is a fundamental bandgap, E_0' is a gap between first two bottommost conduction bands, Δ_0, Δ_0' are the

Table V. The material data for 14×14 ZB Hamiltonian³⁴, d – distance from the point $(\gamma_1'', \gamma_2'', \gamma_3'')$ to the feasibility region Λ_- . The positive values of $\lambda_1''/E, \lambda_2''/E, \lambda_3''/E, \lambda_4''/E$ are printed in bold.

# El ^a	γ_1''	γ_2''	γ_3''	λ_1''/E	λ_2''/E	λ_3''/E	λ_4''/E	d
1 GaAs ^a	0.18	0.42	0.11	-2.49	-1.55	0.98	0.35	0.26
2 GaAs ^b	-0.59	-0.02	-0.34	2.69	-0.34	-0.46	1.55	0.41
3 GaAs ^c	-1.48	-0.03	-0.61	5.23	-0.24	-0.39	3.26	0.87
4 AlAs ^c	-0.91	0.34	-0.31	1.38	-1.39	0.67	2.52	0.67
5 InAs ^c	0.76	0.59	0.12	-3.84	-2.73	0.78	0.05	0.21
6 GaP ^c	-1.55	-0.16	-0.84	7.25	-0.33	-1.31	3.75	1.00
7 AlP ^c	-1.22	0.22	-0.46	3.10	-1.04	0.28	3.04	0.81
8 InP ^d	0.44	0.46	-0.13	-1.49	-2.67	0.08	0.87	0.23
9 InP ^e	-0.50	-0.15	-0.68	5.19	-0.94	-1.85	2.24	0.71
10 InP ^c	-1.54	-0.03	-0.66	5.63	-0.34	-0.50	3.48	0.93
11 GaSb ^c	-0.39	0.59	-0.03	-1.79	-2.04	1.48	1.65	0.44
12 AlSb ^c	-0.99	0.58	-0.32	0.61	-2.31	1.18	3.13	0.84
13 InSb ^c	-2.89	-0.92	-1.61	16.20	1.75	-3.77	5.87	2.23

^a Set 1 from [34] ($\alpha = 0.065$) ^b Set 2 from [34] ($\alpha = 0.085$)

^c Parameters obtained via (23) from the data in [80] and [30]

^d Set 1 from [34] ($\alpha = 0.12$) ^e Set 2 from [34] ($\alpha = 0.2$)

spin-splitting parameters of the valence and conduction bands correspondingly, Q is the interband momentum matrix element (see Fig 1 in 34). For a complete description of the Hamiltonian one additionally needs to define other material dependent parameters $P'_0, \bar{\Delta}, \kappa, C_k$. Those are determined by fitting the bandstructure to experimental data³⁴. For that reason, we are focused only on the sources where the full sets of fitted Hamiltonian parameters have been reported in the context of the considered 14×14 model.

Beside the sets $\gamma_1'', \gamma_2'', \gamma_3''$ from the original paper³⁴, that provides them for GaAs and InP explicitly, we used the parameters sets from J.-M. Jancu et al. [80] and recommended there Luttinger parameters from [30] to calculate the respective values of $\gamma_1'', \gamma_2'', \gamma_3''$ for GaAs, AlAs, InAs, GaP, AlP, InP, GaSb, AlSb and InSb. All calculated parameters along with the results of ellipticity analysis are collected in Table V.

Each of the considered in Table V sets fails two out of four ellipticity constraints except the sets for AlAs, AlP and InSb, for which three ellipticity constraints are violated. For GaAs set 1 from Table V we can confirm a reduction of distance d to the feasibility region Λ_- in the space $\gamma_1'', \gamma_2'', \gamma_3''$ compared to the best of GaAs sets for 6×6 and 8×8 Hamiltonians. This set and set #8 are taken from the original work. Both sets were calculated using cyclotron resonance experiments³⁴. The second pair of sets #2, #9, which are deemed more consistent experimentally⁸¹, is slightly off the region Λ_- ; but the corresponding values of d are within the range of the same-material values of d from Table II. Parameter sets for other materials are even further away from Λ_- than the un-rescaled same-materials sets for 8×8 Hamiltonian.

The observed increase of the distance to Λ_- seems to be theoretically unfounded, especially in the view of for-

mula (3). Recall, that the relative norm⁴⁰ of the perturbative term from (3) should decrease after eigenstates are moved from perturbative class (class B) in to the basis (class A). It can be explained as follows.

In the 8×8 model the influence of valence bands on the CB states was represented directly by the parameters P_0, B and, we suppose, indirectly by the perturbative CB parameter A' . The absence of A' in the CB eigenvalue from (22) suggest that the 14×14 model was derived under assumption that A' depends on the upper CB states only, now included in the basis. In such a situation, all cross-influence between valence and conduction bands are incorporated into P and Q by using fitting to experimental data. Then it is propagated to $\gamma_1'', \gamma_2'', \gamma_3''$ with help of formula (23). But the terms $\gamma_1'', \gamma_2'', \gamma_3''$ in the right-hand side of (23) were fitted to experiments under assumption of the non-zero valence band contribution to A' . That explains why the parameter triplets $\gamma_1'', \gamma_2'', \gamma_3''$ for materials with smaller fundamental bandgap E_0 (InAs, GaSb, InSb) end up having larger d .

On the other hand, the conduction band states in the materials with larger E_0 (AlAs, AlP, AlSb) may in reality be influenced by the higher bands not included in the basis. That influence is assumed to be zero in the model, because CB eigenvalues are equal to E even for the newly included in the basis p -like bands. If non-negligible, the influence is accounted by P, Q and then propagated to $\gamma_1'', \gamma_2'', \gamma_3''$ by the mechanism described above. That explain the increase in d for large-bandgap materials from Table V (AlAs, AlP, AlSb).

For some parameter sets from Table V the ellipticity might be corrected by rescaling of P, Q in a way similar to the rescaling procedure from Section IV. This will, of course, affect the accuracy of bandstructure and therefore must involve the optimization procedure with respect to the parameters P, Q and possibly $\gamma_1'', \gamma_2'', \gamma_3''$, if our hypothesis holds true.

Now we proceed to the second implementation of 14×14 ZB Hamiltonian model. The initial version of this model was derived by U. Rössler using the theory of invariants⁸² and then extended in the work of H. Mayer and U. Rössler⁷³ by adding first-order perturbative corrections to the lowest conduction and upper valence bands. The most recent version of the Hamiltonian was provided by R. Winkler³⁵. It additionally includes the second order conduction-valence band mixing parameters similar to B from Kane Hamiltonian (9).

All three mentioned versions of 14×14 ZB Hamiltonian are connected by the common assumption that six second-order diagonal terms related to the newly added p -like CB states are neutralized by the counter-influence of other bands, e.g. the representation of H_{8c8c}, H_{8c8c} from Table C.5 of [35]. In terms of ellipticity such an assumption results in the presence of zero eigenvalue among the set of eigenvalues of the quadratic form associated with this implementation. Our calculations⁵⁶ confirm that. Therefore, this Hamiltonian is not elliptic by design.

It is worthwhile pointing that, unlike first, the second implementation of 14×14 Hamiltonian^{35,73,82} can be regarded as an extension of Kane model studied in section IV. The Hamiltonian contains the perturbative correction to s -like CB states and the conduction-valence band mixing parameters. So, all inter-band interaction effects embodied in the 8×8 representation³³ can be properly accounted for. In our opinion, two analyzed implementations of the 14×14 Hamiltonian model are less universal material-wise than 8×8 Hamiltonians, despite being more accurate at describing CB related phenomena^{78,79}. For such higher band models, the assumptions regarding the interactions of in-basis conduction band states require a revision.

CONCLUSIONS

We performed a systematic study of ellipticity conditions for 6×6 , 8×8 , 14×14 $k \cdot p$ Hamiltonians in the bulk zinc blende crystals. The conditions take roots in the fundamental axioms of quantum mechanics concerning the description of observable states and properties of Hamiltonian as a differential operator. They appear in the form of constraints on the values of material parameters pertaining to the second-order-in- k terms from the Hamiltonian in the momentum representation.

For 6×6 and 8×8 models we examined an extensive number of parameter sets for GaAs, AlAs, InAs, GaP, AlP, InP, GaSb, AlSb, InSb, GaN, AlN, InN and C that are gathered from the widely accepted sources of reference literature on material parameters²⁹⁻³¹. The results of the performed analysis reaffirm earlier conclusions on the violation of Hamiltonian ellipticity^{16,27} and its cause^{19,41}. Furthermore, we demonstrated that this violation is a much more common problem material-wise. Among all analyzed materials only carbon has parameter sets that make 6×6 Hamiltonians elliptic and therefore admissible from a theoretical point of view. Other sets of material parameters incur violation of one out of four ellipticity constraints: $2\gamma_2 - \gamma_1 + 3\gamma_3 < 0$. This can be traced to a non-negligible influence of conduction bands on the heavy-hole and light-hole, accounted perturbatively in $\gamma_1, \gamma_2, \gamma_3$. We conclude that this model is not accurate enough to describe all considered bands reliably and to remain elliptic at the same time.

The situation becomes more complex for 8×8 Hamiltonians, where the bottom-most conduction band is included into the basis. None of the analyzed parameter sets are admissible, because the conduction-band ellipticity constraint is violated for all sets, when the absence of inversion asymmetry ($B = 0$) is assumed. However, the degree of non-ellipticity in the valence-band part of the Hamiltonian, which we characterize in terms of distance to the feasibility region Λ_- in the space of Luttinger-like parameters, decreases. Several parameter sets for InAs, AlP and AlSb satisfy the ellipticity constraints for the valence-band part. It corroborates the evidence on the

perturbative source of non-ellipticity. We note, that in the case of $B = 0$, these constraints have the same structure as the ellipticity constraints for 6×6 Hamiltonians.

As one possible way to remedy the situation with the lack of ellipticity in the 8×8 model we propose a parameter rescaling procedure. It is based on the idea of adjusting the first-order conduction-valence mixing parameter P_0 to change $A, \gamma'_1, \gamma'_2, \gamma'_3$ and make the Hamiltonian elliptic. The proposed here rescaling procedure accounts for a full set of ellipticity constraints and thus improve the previous approaches^{20,57}, targeted solely at imposing the conduction band constraint $1 + A > 0$.

The results of the rescaling procedure for all materials except InAs, are presented in Table III. Each of the admissible sets is made via (18) from one of the original sets that lead to a minimal absolute difference in the parameter A per material. Notwithstanding the attempt to minimize the effects of rescaling on the bandstructure, these effects are negligible (≤ 11 meV) only for AlP, AlSb, AlAs, InP and GaN (see FIG. 3). They may be considered small (≤ 50 meV) for GaP, InSb, InN and can not be ignored for the rest of materials from the table (see FIG. 4 for visual comparisons). For them, the rescaling leads to a noticeable change in the conduction band dispersion. Heavy hole (HH) and light hole (LH) bands remain visually unaffected even though the differences are non-zero. The rescaling also causes an increase in the curvature of the split-off (SO) band which makes it the main source of total valence-band adjustment error. For all mentioned materials excluding GaP and AlN, the magnitude of this error is proportional to the relative change in E_p . Therefore, in most cases the Hamiltonian based on the new parameters is elliptic, yet incapable of reliably describing the conduction-valence band transition phenomena, except those occurring at the band edge.

In attempt to counter for the observed bandstructure discrepancies and to derive the admissible parameter set for InAs we consider the use of B as an additional adjustment parameter. This requires a generalization of the ellipticity conditions for the 8×8 Hamiltonian to the case of non-zero B . Recall, that, due to the inversion asymmetry, this case is theoretically more relevant to the majority of zinc blende materials. The form of the generalized ellipticity conditions allows us to draw two important conclusions.

First, setting B to some nonzero value will not break ellipticity of 8×8 Hamiltonians if the parameter set – the Hamiltonian is based upon – is admissible with zero B . We use this property to calculate two distinct values of B for the materials. The larger value of B minimizes the error of conduction band and makes the errors in the dispersion of other (most notably SO) bands larger. We left aside a discussion on physical relevance of the calculated values of B and presented the bandstructure plots with $B \neq 0$ for InN only. Our intent here has been to show that B -adjustment can be used to partially correct the bandstructure distorted by rescaling.

Second, the parameter B could not be set to zero for the materials where $1 + A' < 0$ without sacrificing ellipticity of the 8×8 Hamiltonian. At the same time, the adjustment of B can be used to correct the ellipticity of CB part of the Hamiltonian provided that the valence-band ellipticity constraints are fulfilled by $\gamma'_1, \gamma'_2, \gamma'_3$. We discovered four parameter sets for InAs, AlP, AlSb where this is true. These parameter sets are highly regarded as overall physically consistent³⁰. Four minimally admissible values of B that complement each of the mentioned sets to make the Hamiltonian elliptic, are collected in Table IV.

Besides being the source of admissible B , the data from Table IV illustrates that the admissible sets obtained by the rescaling procedure are not the best option in terms of the bandstructure fit, at least for AlP. We postulate that there exist admissible parameters of 8×8 Hamiltonian³³ better in terms of bandstructure error for other materials too. To find them one should fit the Hamiltonian bands' dispersions to the spin-resolved bandstructure by adjusting the entire set of the Hamiltonians parameters simultaneously and by using the ellipticity conditions as constraints for the fit. This idea is supplemented by the fact, that the ellipticity region in the space of parameters that satisfy the constraints is convex and connected. The results of such fitting procedure will be also useful to quantify the limits of this and other $k \cdot p$ models, assuming that the bandstructure used as a fitting target is reliable⁸³. This would constitute an important for the future studies.

Finally, we analyzed two popular implementations of the 14×14 ZB Hamiltonian model^{34,35}. The ellipticity of the first implementation is described by precisely the same set of constraints as for the 6×6 model, but written in terms of the reduced Luttinger-like parameters $\gamma''_1, \gamma''_2, \gamma''_3$. Unfortunately, the parameter analysis shows that none of the available sets for a studied list of materials is admissible in terms of the Hamiltonian ellipticity. We conclude that an overly-strict set of assumptions regarding the perturbative influence of outer bands on the model's conduction bands is to be responsible for the lack of ellipticity. The second analysed 14×14 Hamiltonian is more general in that regard. It is however non-elliptic by design owing to the fact that the second-order-in- k terms are zero for three upper p -like conduction bands.

Based on the supplied evidence we surmise that both 14×14 implementations are less universal than the previously studied 8×8 Hamiltonian. The revision of indicated

assumptions and, perhaps, some unifications are necessary to bring these extended models to a strict theoretical ground.

The analysis conducted in this paper covers possible extensions of the considered models, such as the inclusion strain-stress, electromagnetic or other phenomena, as long as such extensions do not change the structure of second-order-in- k terms of the Hamiltonian. The analysis can be easily transferred to the cases when momentum quantization is applied in one- or two- dimensions (quantum wells, wires, etc). It can also be applied to the materials, that are intrinsically non-three dimensional (non-3D), like graphene, silicene or others; especially given that many high-accuracy bandstructure diagrams for those kind of materials are readily available⁸⁴⁻⁸⁶.

We note that ellipticity conditions stated here are not valid for anything other than the considered three dimensional $k \cdot p$ Hamiltonians for ZB crystals. The whole analysis will have to be repeated in each specific non-3D case.

The applications to materials with other-than-zinc-blende crystal structures are also possible. The Hamiltonian parameters for ternary alloys, for instance, are typically calculated by using a linear combination of the parameters for the constituents. Therefore the alloys' parameters will be elliptic if the parameters of constituents are, because the ellipticity region is connected and convex in the space of parameters. Similar reasoning can be applied to the calculation of time-dependent Hamiltonian parameters with help of the Varshni formulas. There might be some complications with analytic calculation of quadratic form's eigenvalues, for more complicated Hamiltonians with different symmetry-structure. This is not a major issue, because for any specific material the ellipticity of $k \cdot p$ Hamiltonian can also be verified numerically.

ACKNOWLEDGEMENTS

The first author acknowledges the partial financial support from The Royal Society of Canada via 2017 RSC-Ukraine exchange program. Both authors are grateful to Dr. Sunil Patil for our earlier discussions on the topic. The support of NSERC and the CRC Program is also acknowledged.

* sytnikd@gmail.com

† rmelnik@wlu.ca

¹ J. M. Luttinger and W. Kohn, Phys. Rev. **97**, 869 (1955).

² E. O. Kane, Journal of Physics and Chemistry of Solids **1**, 249

³ S. Prabhakar, R. V. Melnik, P. Neittaanmäki, and T. Tiihonen, Journal of Computational and Theoretical Nanoscience **10**, 534 (2013).

⁴ S. Prabhakar, R. V. Melnik, P. Neittaanmäki, and T. Tiihonen, Physica E: Low-dimensional Systems and Nanostructures **46**, 97 (2012).

⁵ (1953). Xia, Phys. Rev. B **43**, 9856 (1991).

⁶ S. Prabhakar, R. Melnik, and L. L. Bonilla, Journal of Applied Physics **113**, 244306 (2013).

- ⁷ M. Alvaro, L. Bonilla, M. Carretero, R. Melnik, and S. Prabhakar, *Journal of Physics: Condensed Matter* **25**, 335301 (2013).
- ⁸ S. R. Patil and R. V. N. Melnik, *Nanotechnology* **20**, 125402 (13pp) (2009).
- ⁹ F. J. G. de Abajo, *Reviews of Modern Physics* **79**, 1267 (2007).
- ¹⁰ S. L. Chuang, *Wiley series in pure and applied optics* (Wiley, New York, 1995) p. 736.
- ¹¹ S. L. Chuang, *Physics of photonic devices* (John Wiley & Sons, Hoboken, N.J., 2009) p. 821.
- ¹² D. L. Smith and C. Mailhot, *Phys. Rev. B* **33**, 8345 (1986).
- ¹³ F. Szmulowicz, *Phys. Rev. B* **54**, 11539 (1996).
- ¹⁴ B. A. Foreman, *Phys. Rev. B* **75**, 235331 (2007).
- ¹⁵ W. Yang and K. Chang, *Phys. Rev. B* **72**, 233309 (2005).
- ¹⁶ R. G. Veprek, S. Steiger, and B. Witzigmann, *Phys. Rev. B* **76**, 165320 (2007).
- ¹⁷ R. G. Veprek, S. Steiger, and B. Witzigmann, *Journal of Computational Electronics* **7**, 521 (2008).
- ¹⁸ B. Lassen, R. Melnik, and M. Willatzen, *Commun. Comput. Phys.* **6**, 699 (2009).
- ¹⁹ D. Sytnyk, S. Patil, and R. Melnik, *ArXiv e-prints* (2010), arXiv:1004.4152 [cond-mat.mtrl-sci].
- ²⁰ B. A. Foreman, *Phys. Rev. B* **56**, R12748 (1997).
- ²¹ X. Cartoixa, Soler, *Theoretical methods for spintronics in semiconductors with applications*, Ph.D. thesis, California Institute of Technology (2003).
- ²² K. I. Kolokolov, J. Li, and C. Z. Ning, *Phys. Rev. B* **68**, 161308 (2003).
- ²³ R. Eppenga, M. F. H. Schuurmans, and S. Colak, *Phys. Rev. B* **36**, 1554 (1987).
- ²⁴ M. V. Kisin, B. L. Gelmont, and S. Luryi, *Phys. Rev. B* **58**, 4605 (1998).
- ²⁵ T. Eissfeller and P. Vogl, *Phys. Rev. B* **84**, 195122 (2011).
- ²⁶ V. Berestetskii, E. Lifshitz, and L. Pitaevskii, *Quantum Electrodynamics*, 2nd ed., *Course of Theoretical Physics*, Vol. 4 (Pergamon Press, 1982).
- ²⁷ R. G. Veprek, S. Steiger, and B. Witzigmann, *Opt. Quantum. Electron.* (2009), 10.1007/s11082-008-9259-9.
- ²⁸ P. Lawaetz, *Phys. Rev. B* **4**, 3460 (1971).
- ²⁹ O. Madelung, U. Rössler, and M. Schulz, *Group IV Elements, IV-IV and III-V Compounds. Part b* - Landolt-Börnstein - Group III Condensed Matter Numerical Data and Functional Relationships in Science and Technology, Vol. 41A1b (Springer-Verlag, 2002).
- ³⁰ I. Vurgaftman, J. R. Meyer, and L. R. Ram-Mohan, *Journal of Applied Physics* **89**, 5815 (2001), <https://doi.org/10.1063/1.1368156>.
- ³¹ O. Madelung, *Semiconductors : data handbook* (Springer, Berlin ; New York, 2004) p. 691.
- ³² P. Rinke, M. Winkelnkemper, A. Qteish, D. Bimberg, J. Neugebauer, and M. Scheffler, *Phys. Rev. B* **77**, 075202 (2008).
- ³³ T. B. Bahder, *Phys. Rev. B* **41**, 11992 (1990).
- ³⁴ P. Pfeffer and W. Zawadzki, *Phys. Rev. B* **53**, 12813 (1996).
- ³⁵ R. Winkler, *Spin-orbit coupling effects in two-dimensional electron systems* (Springer, Berlin; New York, 2003) p. 238.
- ³⁶ E. O. Kane, "Energy band theory," (Notrth-Holland, 1982) Chap. 4A, pp. 193–216.
- ³⁷ L. Voon and M. Willatzen, *The k p Method: Electronic Properties of Semiconductors* (Springer Science+Business Media, 2009).
- ³⁸ G. Bir and G. Pikus, *Symmetry and Strain-Induced Effects in Semiconductors* (Wiley, New York, 1974) p. 484, translated from Russian by P. Shelnitz.
- ³⁹ J. M. Luttinger, *Phys. Rev.* **102**, 1030 (1956).
- ⁴⁰ T. Kato, *Perturbation theory for linear operators.* (Grundlehren der mathematischen Wissenschaften. Band 132. Berlin-Heidelberg-New York: Springer-Verlag. xx, 592 p. with 3 figures DM 79.20, 1966).
- ⁴¹ D. Sytnyk, *Mathematical modeling of quantum dots with generalized envelope functions approximations and coupled partial differential equations*, Master's thesis, Wilfrid Laurier University (Canada) (2010).
- ⁴² P. Pfeffer and W. Zawadzki, *Phys. Rev. B* **41**, 1561 (1990).
- ⁴³ S. I. Dorozhkin, *JETP Lett.* **88**, 819 (2008).
- ⁴⁴ L. E. Ballentine, *Quantum mechanics: a modern development* (World Scientific, Singapore, 2006) p. 672.
- ⁴⁵ P. A. M. Dirac, *The principles of quantum mechanics* (Clarendon Press, Oxford, UK, 1981) p. 340.
- ⁴⁶ G. Teschl, *Mathematical methods in quantum mechanics*, Graduate Studies in Mathematics, Vol. 99 (American Mathematical Society, Providence, RI, 2009) pp. xiv+305, with applications to Schrödinger operators.
- ⁴⁷ M. G. Burt, *J. Phys.: Condens. Matter* **11**, 53 (1999), 53.
- ⁴⁸ L. Hörmander, *The analysis of linear partial differential operators. II: Differential operators with constant coefficients.* (Springer-Verlag: Berlin Heidelberg-NewYork - Tokyo, 1983).
- ⁴⁹ Y. Egorov and M. Shubin, *Foundations of the classical theory of partial differential equations. Transl. from the Russian by R. Cooke. 2nd printing of the 1st ed. 1992.* (Berlin: Springer, 1998) p. 259.
- ⁵⁰ L. Hörmander, *The analysis of linear partial differential operators. I: Distribution theory and Fourier analysis.* (Springer-Verlag: Berlin Heidelberg-NewYork - Tokyo, 1983).
- ⁵¹ P. Yu and M. Cardona, *Fundamentals of semiconductors: physics and materials properties*, 3rd ed. (Springer, 2005) p. 639.
- ⁵² R. Courant and P. D. Lax, *Proc. Natl. Acad. Sci. U. S. A.* **42**, 872 (1956).
- ⁵³ R. G. Veprek, D. Walechka, and B. Witzigmann, *Electronic Transport, Optical and Other Properties* - Landolt-Börnstein - Group III Condensed Matter Numerical Data and Functional Relationships in Science and Technology, Vol. 41A1b (Springer-Verlag, 2002).
- ⁵⁴ C. R. Pidgeon and R. N. Brown, *Phys. Rev.* **146**, 575 (1966).
- ⁵⁵ M. Cardona, N. Christensen, M. Dobrowolska, J. Furdyna, and S. Rodriguez, *Solid State Communications* **60**, 17 (1986).
- ⁵⁶ All computations were performed in Maple. Codes are available at www.imath.kiev.ua/~sytnyk/projects/kp.
- ⁵⁷ S. Birner, in *Multi-Band Effective Mass Approximations* (Springer, 2014) pp. 193–244.
- ⁵⁸ C. M. O. Bastos, F. P. Sabino, P. E. F. Junior, T. Campos, J. L. F. D. Silva, and G. M. Sipahi, *Semiconductor Science and Technology* **31**, 105002 (2016).
- ⁵⁹ G. Dresselhaus, A. F. Kip, and C. Kittel, *Phys. Rev.* **98**, 868 (1955).
- ⁶⁰ I. Vurgaftman and J. R. Meyer, *Journal of Applied Physics* **94**, 3675 (2003), <https://doi.org/10.1063/1.1600519>.
- ⁶¹ F. Issiki, S. Fukatsu, and Y. Shiraki, *Applied Physics Letters* **67**, 1048 (1995), <https://doi.org/10.1063/1.114460>.

- ⁶² F. Viñas, H. Q. Xu, and M. Leijnse, *Phys. Rev. B* **95**, 115420 (2017).
- ⁶³ S. Birner, T. Zibold, T. Andlauer, T. Kubis, M. Sabathil, A. Trellakis, and P. Vogl, *IEEE Transactions on Electron Devices* **54**, 2137 (2007).
- ⁶⁴ Z. Zhang, R. Zhang, B. Liu, Z. Xie, X. Xiu, P. Han, H. Lu, Y. Zheng, Y. Chen, C. Tang, *et al.*, *Solid State Communications* **145**, 159 (2008).
- ⁶⁵ F. Mei, N. Tang, X. Wang, J. Duan, S. Zhang, Y. Chen, W. Ge, and B. Shen, *Applied Physics Letters* **101**, 132404 (2012).
- ⁶⁶ R. Eppenga and M. F. H. Schuurmans, *Phys. Rev. B* **37**, 10923 (1988).
- ⁶⁷ B. Jusserand, D. Richards, G. Allan, C. Priester, and B. Etienne, *Phys. Rev. B* **51**, 4707 (1995).
- ⁶⁸ D. Richards, B. Jusserand, G. Allan, C. Priester, and B. Etienne, *Solid-State Electronics* **40**, 127 (1996), proceedings of the Seventh International Conference on Modulated Semiconductor Structures.
- ⁶⁹ A. N. Chantis, M. Cardona, N. E. Christensen, D. L. Smith, M. van Schilfgaarde, T. Kotani, A. Svane, and R. C. Albers, *Phys. Rev. B* **78**, 075208 (2008).
- ⁷⁰ A. N. Chantis, N. E. Christensen, A. Svane, and M. Cardona, *Phys. Rev. B* **81**, 205205 (2010).
- ⁷¹ M. Braun and U. Rössler, *Journal of Physics C: Solid State Physics* **18**, 3365 (1985).
- ⁷² W. Zawadzki, P. Pfeffer, and H. Sigg, *Solid State Communications* **53**, 777 (1985).
- ⁷³ H. Mayer and U. Rössler, *Phys. Rev. B* **44**, 9048 (1991).
- ⁷⁴ W. Zawadzki, I. T. Yoon, C. L. Littler, X. N. Song, and P. Pfeffer, *Phys. Rev. B* **46**, 9469 (1992).
- ⁷⁵ P. Pfeffer and W. Zawadzki, *Phys. Rev. B* **74**, 233303 (2006).
- ⁷⁶ N. Cavassilas, F. Aniel, K. Boujdaria, and G. Fishman, *Phys. Rev. B* **64**, 115207 (2001).
- ⁷⁷ R. D. R. Bhat, P. Nemeč, Y. Kerachian, H. M. van Driel, J. E. Sipe, and A. L. Smirl, *Phys. Rev. B* **71**, 035209 (2005).
- ⁷⁸ M. El kurdi, G. Fishman, S. Sauvage, and P. Boucaud, *Phys. Rev. B* **68**, 165333 (2003).
- ⁷⁹ M. Gladysiewicz, R. Kudrawiec, and M. S. Wartak, *Journal of Applied Physics* **118**, 055702 (2015), <https://doi.org/10.1063/1.4927922>.
- ⁸⁰ J.-M. Jancu, R. Scholz, E. A. de Andrada e Silva, and G. C. La Rocca, *Phys. Rev. B* **72**, 193201 (2005).
- ⁸¹ I. Gorczyca, P. Pfeffer, and W. Zawadzki, *Semiconductor Science and Technology* **6**, 963 (1991).
- ⁸² U. Rössler, *Solid State Communications* **49**, 943 (1984).
- ⁸³ T. Okuda, *Journal of Physics: Condensed Matter* **29**, 483001 (2017).
- ⁸⁴ D. Massatt, S. Carr, M. Luskin, and C. Ortner, *Multiscale Modeling & Simulation* **16**, 429 (2018).
- ⁸⁵ H. Pan, Z. Li, C.-C. Liu, G. Zhu, Z. Qiao, and Y. Yao, *Physical review letters* **112**, 106802 (2014).
- ⁸⁶ W. Lin, J. Li, W. Wang, S.-D. Liang, and D.-X. Yao, *Scientific reports* **8**, 1674 (2018).